International Journal of Bifurcation and Chaos, Vol. 14, No. 8 (2004) 2525–2553
© World Scientific Publishing Company

ENVELOPING SURFACES AND ADMISSIBLE VELOCITIES OF HEAVY RIGID BODIES

IGOR N. GASHENENKO
Institute of Applied Mathematics and Mechanics of NAS of Ukraine,
Luxemburg Str. 74, Donetsk 83114, Ukraine
gashenenko@iamm.ac.donetsk.ua

PETER H. RICHTER
Institut für Theoretische Physik, University of Bremen,
Postfach 330 440, 28334 Bremen, Germany
prichter@physik.uni-bremen.de

Received March 11, 2003; Revised August 8, 2003

The general Euler-Poisson problem of rigid body motion is investigated. We study the three-dimensional algebraic level surfaces of the first integrals, and their topological bifurcations. The main result of this article is an analytical and qualitatively complete description of the projections of these integral manifolds to the body-fixed space of angular velocities. We classify the possible types of these invariant sets and analyze the dependence of their topology on the parameters of the body and the constants of the first integrals. Particular emphasis is given to the enveloping surfaces of the sets of admissible angular velocities. Their pre-images in the reduced phase space induce a Heegaard splitting which lends itself for a general choice of complete Poincaré surfaces of section, irrespective of whether or not the system is integrable.

Keywords: Rigid body dynamics; bifurcation set; invariant manifolds; angular velocity.

1. Introduction

The motion of rigid bodies is one of the more challenging topics in courses on classical mechanics, see the textbook by Landau and Lifshitz [1958] for an introduction. In these courses students are given the impression that there are just two families of problems: *Euler's* case of an asymmetric rigid body fixed at its center of gravity, and the *Lagrange* case of a symmetric body in a gravitational field, fixed to a point on its symmetry axis (the "heavy spinning top"). The integration of the corresponding equations of motion is possible in terms of elliptic functions. It is not usually mentioned, however, that the vast majority of problems — motion of a rigid body, with one point held fixed, in a gravity field pointing in the direction $\boldsymbol{\gamma}$ — is *not integrable*. The configuration space SO(3) has three degrees of freedom (e.g. the Euler angles), but as a rule, energy h and the vertical component $l = \langle \mathbf{l}, \boldsymbol{\gamma} \rangle$ of the angular momentum vector $\mathbf{l}$ are the only constants of motion. Euler's case is special in that $\langle \mathbf{l}, \mathbf{l} \rangle =: g^2$ is a third, independent integral, and in Lagrange's case the third integral $\langle \mathbf{l}, \mathbf{r} \rangle =: l_s$ derives from the symmetry with respect to rotation about the body's axis; here $\mathbf{r}$ is the vector connecting the fixed point to the center of mass.

Traditionally, the equations of motion are written in the Euler–Poisson form [Arnold, 1974]

$$A\dot{\boldsymbol{\omega}} = A\boldsymbol{\omega} \times \boldsymbol{\omega} - \boldsymbol{\gamma} \times \mathbf{r}\,, \quad \dot{\boldsymbol{\gamma}} = \boldsymbol{\gamma} \times \boldsymbol{\omega}\,, \qquad (1)$$

where the angular velocity vector $\boldsymbol{\omega} = (\omega_1, \omega_2, \omega_3) \in \mathbb{R}^3$ and the direction of gravity $\boldsymbol{\gamma} = (\gamma_1, \gamma_2, \gamma_3) \in \mathbb{R}^3$, both viewed from the body fixed coordinate system of principal axes

$(\mathbf{e}_1, \mathbf{e}_2, \mathbf{e}_3)$, are considered as phase space variables. The three components of the tensor of inertia $A = \mathrm{diag}(A_1, A_2, A_3)$, and the three components of the center of mass vector $\mathbf{r} = (r_1, r_2, r_3) \in \mathbb{R}^3$ are fixed parameters. The angular momentum and angular velocity are related by the identity $\mathbf{l} = A\boldsymbol{\omega}$.

1.1. *Energy surfaces and their bifurcations*

The six-dimensional phase space $\mathbb{R}^3(\boldsymbol{\omega}) \times \mathbb{R}^3(\boldsymbol{\gamma})$ is effectively only four-dimensional because Eqs. (1) have two "geometric" constants, or *Casimir constants*. One is the length of the vector $\boldsymbol{\gamma}$; hence we may stick with the *Poisson sphere* $S^2(\boldsymbol{\gamma})$, defined by $\langle \boldsymbol{\gamma}, \boldsymbol{\gamma} \rangle = 1$. The other Casimir constant is $\langle A\boldsymbol{\omega}, \boldsymbol{\gamma} \rangle = \langle \mathbf{l}, \boldsymbol{\gamma} \rangle = l$. As a consequence of these two restrictions, the Euler–Poisson equations describe motion in the four-dimensional cotangent bundle of the Poisson sphere which is also called the *reduced phase space*. From a practical point of view, it is convenient to consider this phase space as embedded in $\mathbb{R}^3(\boldsymbol{\omega}) \times \mathbb{R}^3(\boldsymbol{\gamma})$, and to treat $L = \langle \mathbf{l}, \boldsymbol{\gamma} \rangle$ and $I = \langle \boldsymbol{\gamma}, \boldsymbol{\gamma} \rangle$ as integrals with constant values l and 1, respectively. Together with the energy integral, we have three general constants of motion,

$$
\begin{gathered}
H = \frac{1}{2} \langle A\boldsymbol{\omega}, \boldsymbol{\omega} \rangle - \langle \boldsymbol{\gamma}, \mathbf{r} \rangle = h \,, \\
L = \langle A\boldsymbol{\omega}, \boldsymbol{\gamma} \rangle = l \,, \quad I = \langle \boldsymbol{\gamma}, \boldsymbol{\gamma} \rangle = 1 \,.
\end{gathered} \tag{2}
$$

Each pair of values (h, l) defines a three-dimensional compact subset of phase space,

$$
\begin{aligned}
\mathcal{E}^3_{h,l} &= \{H = h, L = l, I = 1\} \\
&\subset \mathbb{R}^3(\boldsymbol{\omega}) \times \mathbb{R}^3(\boldsymbol{\gamma}) \,,
\end{aligned} \tag{3}
$$

which is invariant with respect to the phase flow. The set $\mathcal{E}^3_{h,l}$ is called a *energy surface* of the system. For most values (h, l), the energy surface is a smooth manifold; the exception are values (h, l) for which $\mathcal{E}^3_{h,l}$ contains points $(\boldsymbol{\omega}, \boldsymbol{\gamma})$ where the *momentum map* $\mathcal{F} : (\boldsymbol{\omega}, \boldsymbol{\gamma}) \mapsto (h, l)$ is singular, $\mathrm{rank}(d\mathcal{F}) < 2$. The corresponding set of *critical values* (h, l) is called the *bifurcation set* Σ of the energy surface, for the given parameters A and $\mathbf{r}$. When (h, l) is varied across the bifurcation set, the topological type of $\mathcal{E}^3_{h,l}$ changes.[1]

A systematic way for finding points $(\boldsymbol{\omega}, \boldsymbol{\gamma})$ where the momentum map is critical, is to look for situations where the equations

$$
\begin{aligned}
\frac{\partial(H - \mu_1 L - \mu_2 I)}{\partial \boldsymbol{\omega}} &= 0 \,, \\
\frac{\partial(H - \mu_1 L - \mu_2 I)}{\partial \boldsymbol{\gamma}} &= 0 \,,
\end{aligned} \tag{4}
$$

allow for real solutions μ_1, μ_2. From the first equation we infer that $\boldsymbol{\gamma}$ and $\boldsymbol{\omega}$ must be collinear, hence $\dot{\boldsymbol{\gamma}} = 0$. Using the second equation it is straightforward to show that also $\dot{\boldsymbol{\omega}} = 0$. Thus we see that the bifurcation set of the energy surface consists of values (h, l) where the Euler–Poisson equations have stationary solutions, or *relative equilibria*.

Notice that Eqs. (1) do not describe the body's rotation about the space fixed vertical axis. The corresponding angle φ is a S^1-symmetry of the full system and has been separated. It is obtained by integration of

$$
\dot{\varphi} = \frac{\gamma_1 \omega_1 + \gamma_2 \omega_2}{\gamma_1^2 + \gamma_2^2} \,, \tag{5}
$$

once the solutions of (1) have been determined. Relative equilibria are steady rotations $\dot{\varphi} = \mathrm{const}$ about the vertical axis.

As usual in connection with the separation of an angular variable, the part of the kinetic energy which is associated with the φ-motion, $l^2/2\langle A\boldsymbol{\gamma}, \boldsymbol{\gamma} \rangle$, depends only on the configurational variables. It is called the "centrifugal potential". Together with the gravitational potential it defines the *effective potential*

$$
U_l = \frac{l^2}{2\langle A\boldsymbol{\gamma}, \boldsymbol{\gamma} \rangle} - \langle \mathbf{r}, \boldsymbol{\gamma} \rangle \,, \tag{6}
$$

of the reduced system. It was proven in [Tatarinov, 1973] that the relative equilibria are in one-to-one correspondence with the critical points of the effective potential U_l.

The tensor of inertia A and center of mass positions $\mathbf{r}$ define a six-dimensional set, but one of the r_i may be used for scaling lengths, and one of the A_i for scaling time (or energy). Unless $\mathbf{r} = 0$ and $A_1 = 0$, we adopt the conventions $|\mathbf{r}| = 1$ and $A = \mathrm{diag}(1, \alpha, \beta)$. Hence the set P of essential parameters is four-dimensional. Remember that the moments of inertia are restricted by $\alpha + \beta > 1$, $\alpha + 1 > \beta$, $\beta + 1 > \alpha$, see Fig. 13.

[1] In the three special cases (Euler, Lagrange, Kovalevskaya) where a third integral $J = j$ exists, the momentum map has a three-dimensional range $\mathbb{R}^3(h, l, j)$, and the bifurcation analysis becomes more involved, see [Dullin, 1994; Richter *et al.*, 1997] for details on the Kovalevskaya case.

Euler's case, $\mathbf{r} = 0$ and $A = (1, \alpha, \beta)$, defines a two-dimensional subset of P. Lagrange's case may be characterized as $\mathbf{e} = (1, 0, 0)$ and $\alpha = \beta > 1/2$, which defines a one-dimensional subset of P. There exists one additional integrable case, the famous Kovalevskaya top [Kowalevski, 1890] where $A = (1, 1, \frac{1}{2})$ and $\mathbf{r} = (\cos\varepsilon, \sin\varepsilon, 0)$; this is again a one-dimensional subset of the four-dimensional parameter space (but $\varepsilon = 0$ is no restriction due to the symmetry in A, hence there is really only *one* Kovalevskaya top).

For all other sets of values A and $\mathbf{r}$, the Euler–Poisson equations are nonintegrable, except for special values of (h, l). This was established in a long series of investigations, going back to Poincaré's seminal book [Poincaré, 1892, Vol. 1, Chap. V, Sec. 86]. Important results in this line of research were obtained by Lyapunov [1954] who demonstrated the nonexistence of general solutions in terms of single-valued functions of time, except for the three known integrable cases; by Husson and Liouville [Arkhangelskii, 1977] who proved the nonexistence of new algebraic integrals if h and l are arbitrary constants; by Kozlov [1980, 1995] who established the nonexistence of new analytical integrals via perturbation of the Euler case; by Dovbysh [1990] who showed the same for perturbations of the Lagrange case; and by Ziglin [1983] who demonstrated the nonexistence of integrals in terms of meromorphic functions of the phase variables. All these results cover only certain aspects of the general problem. Kozlov [1995] had characterized the situation as follows: "For the time being, the question concerning the existence of an additional integral of the equations of rotation of a heavy rigid body (in the real domain and for an arbitrary distribution of masses) remains open."

Nevertheless, a number of invariant features can be identified for the dynamical system (1). As mentioned already, the reduced phase space at given l is foliated by three-dimensional surfaces $\mathcal{E}^3_{h,l}$ of constant energy. As their topological structure changes in connection with relative equilibria, see Appendix 5C in [Arnold, 1974] and Sec. 3.3.4 in [Arnold *et al.*, 1985], it is important to have a survey on these special types of motion. The study of this problem was initiated by Iacob [1971], Katok [1972], and Tatarinov [1974], and will be extended in Sec. 2 below. The projections of $\mathcal{E}^3_{h,l}$ to the Poisson sphere $S^2(\boldsymbol{\gamma})$ and to the space $\mathbb{R}^3(\boldsymbol{\omega})$ of angular velocities are related invariant features; they will be denoted as $\mathcal{U}_{h,l}$ and $\mathcal{V}_{h,l}$, respectively. $\mathcal{U}_{h,l}$ is the set of accessible points $\boldsymbol{\gamma}$ for given (h, l),

$$\mathcal{U}_{h,l} = \{U_l(\boldsymbol{\gamma}) \le h\} \subset S^2(\boldsymbol{\gamma})\,. \tag{7}$$

Its topological nature is used to determine the topology of $\mathcal{E}^3_{h,l}$. The sets $\mathcal{V}_{h,l}$, and their *enveloping surfaces* $\partial\mathcal{V}_{h,l}$, are the main subject of this paper; to our knowledge, these objects have not been studied before in generality. Our results are presented in Sec. 6.

As shown in Secs. 3 and 4, the surfaces $\partial\mathcal{V}_{h,l}$ are projections to $\boldsymbol{\omega}$-space of the two-dimensional sets $\mathcal{P}^2_{h,l}$, defined by local extrema of the squared angular momentum,

$$\mathcal{P}^2_{h,l} = \left\{\frac{d\mathbf{l}^2}{dt} = 0\right\} \subset \mathcal{E}^3_{h,l}\,. \tag{8}$$

Since $\mathbf{l}^2$ is a bounded function on $\mathcal{E}^3_{h,l}$ this condition defines a complete Poincaré surface of section in the sense of [Dullin & Wittek, 1995]. It divides the energy surface into disjoint parts with increasing and decreasing $\mathbf{l}^2$, and the phase space flow keeps changing between the two[2] through intersections with $\mathcal{P}^2_{h,l}$. Hence, irrespective of whether or not the Euler–Poisson equations are integrable, the surfaces $\mathcal{P}^2_{h,l}$ provide a convenient setting for the definition of Poincaré maps. Their projections $\tilde{\mathcal{U}}_{h,l}$ to $\boldsymbol{\gamma}$-space, and $\partial\mathcal{V}_{h,l}$ to $\boldsymbol{\omega}$-space, are also convenient because Propositions 4.1 and 6.1 establish the following nice properties: except at points $\boldsymbol{\gamma} = \pm\mathbf{r}/|\mathbf{r}|$, the projection $\mathcal{P}^2_{h,l} \to \tilde{\mathcal{U}}_{h,l}$ is 2:1, while the projection $\mathcal{P}^2_{h,l} \to \partial\mathcal{V}_{h,l}$ is 1:1 except where $A\boldsymbol{\omega}$ is collinear with $\mathbf{r}$. The two sheets of the projection to $\mathcal{U}_{h,l}$ must be distinguished, as usual in Poincaré maps, by an extra condition; here this could be the choice of sign of $d^2\mathbf{l}^2/dt^2$. Remark: in neither projection is the Poincaré map area preserving, but this does not affect its usefulness.

From these considerations it should be clear that the surfaces $\mathcal{P}^2_{h,l}$ are of particular interest for a general study of rigid body dynamics. Their bifurcation sets $\tilde{\Sigma}$ are therefore of central concern in the present paper. The extra condition in (8) makes $\tilde{\Sigma}$ richer than the bifurcation set Σ of $\mathcal{E}^3_{h,l}$. We show in Sec. 4 that $\tilde{\Sigma}$ contains Σ and, in addition, the lines defined in (31) and (33). Note, however, that

[2]The Euler case is an exception because $\mathbf{l}^2$ is a constant of the motion.

these lines contribute a nonempty difference $\tilde{\Sigma}\backslash\Sigma$ only if the center of gravity $\mathbf{r}$ does not lie on one of the principal axes.

The projections $\tilde{\mathcal{U}}_{h,l}$ are singular at points $\boldsymbol{\gamma} = \pm\mathbf{r}/|\mathbf{r}|$, and $\partial\mathcal{V}_{h,l}$ at points where the angular momentum is collinear with $\mathbf{r}$. This induces artificial bifurcations in the projections when the number of singular points changes, see (49).

As an introduction to the main part of the paper, we discuss the familiar cases of Euler and Lagrange, without paying much attention to their "extra integrals" g^2 or l_s. Of course, some of the more delicate features are lacking in these cases; there is no difference between Σ and $\tilde{\Sigma}$, or between $\mathcal{U}_{h,l}$ and $\tilde{\mathcal{U}}_{h,l}$. In Euler's case there is even no distinction between $\mathcal{V}_{h,l}$ and $\partial\mathcal{V}_{h,l}$. Nevertheless, a study of these cases helps develop an understanding for the new view on rigid body dynamics.

1.2. *Euler's case*

With $\mathbf{r} = 0$ the effective potential is simply

$$U_l = \frac{l^2}{2\langle A\boldsymbol{\gamma}, \boldsymbol{\gamma}\rangle}\,. \tag{9}$$

The middle part of Fig. 1 gives an illustration in terms of colors: low values of U_l in the yellow region, high values in the green. The critical points of $U_l(\boldsymbol{\gamma})$ are easily determined (we assume $A_1 > A_2 > A_3$): minima $U_l = l^2/2A_1$ at $\boldsymbol{\gamma} = \pm\mathbf{e}_1$, saddle points at $\boldsymbol{\gamma} = \pm\mathbf{e}_2$ with $U_l = l^2/2A_2$, maxima $U_l = l^2/2A_3$ at $\boldsymbol{\gamma} = \pm\mathbf{e}_3$. The black graph in the right part of the figure is a schematic representation of the potential. Each point corresponds to one equipotential line, and the graph shows how they are related (such graphs are called *Reeb graphs* [Bolsinov & Fomenko, 1999]); energy increasing from bottom to top, the two branches of level lines in the yellow region join at the separatrix and turn into two green branches.

The left part of Fig. 1 shows the $l \geq 0$ half of the bifurcation diagram (for $l \leq 0$ one gets the mirror image of this picture; the line $l = 0$ is not a critical line). The critical lines $h_i = l^2/2A_i$ separate regions with different topology of $\mathcal{E}^3_{h,l}$. No motion is possible for energies smaller than $l^2/2A_1$. The line $h = l^2/2A_1$ corresponds to two stable steady rotations: both with $\mathbf{l}$ pointing in the $\boldsymbol{\gamma}$-direction, $g^2 = l^2$, but $\mathbf{l} = l\mathbf{e}_1$ in one case, $\mathbf{l} = -l\mathbf{e}_1$ in the other. As h increases at constant l, two (yellow) disks of $\boldsymbol{\gamma}$-values around $\pm\mathbf{e}_1$ become admissible. For each interior point of these disks, the kinetic energy of the reduced system defines an S^1-manifold as admissible end points of vectors $\boldsymbol{\omega}$; on the boundaries $h = U_l(\boldsymbol{\gamma})$, the only possibility for $\boldsymbol{\omega}$ is to be collinear with $\boldsymbol{\gamma}$. We conclude that $\mathcal{E}^3_{h,l}$ consists of two disjoint fiber bundles with disks $D^2 \sim S^2\backslash D^2$ as their bases and circles as fibers, shrinking to points at the boundaries of the disks. This is characteristic of three-spheres, hence $\mathcal{E}^3_{h,l} \sim 2S^3$, cf. [Smale, 1970; Bolsinov *et al.*, 1996] for this kind of reasoning.

When energy increases beyond h_2, with maximum level of U_l in the green region, the accessible part of the Poisson sphere is an annulus $D^2\backslash D^2 \sim S^2\backslash 2D^2$, the corresponding topological type of the energy surface $S^1 \times S^2$. Finally, for $h > h_3$, the entire $\boldsymbol{\gamma}$-sphere S^2 is accessible, and since every $\boldsymbol{\gamma}$ carries a fiber of type S^1, the energy surface is a Poincaré sphere, or the projective space $\mathbb{R}P^3$.

Once the energy surfaces are determined from their projections to $S^2(\boldsymbol{\gamma})$, we may also ask for their projections $\mathcal{V}_{h,l}$ to the space $\mathbb{R}^3(\boldsymbol{\omega})$. This is especially easy in the Euler case where the $\boldsymbol{\omega}$-equation $A\dot{\boldsymbol{\omega}} = A\boldsymbol{\omega} \times \boldsymbol{\omega}$ is independent of the $\boldsymbol{\gamma}$-motion

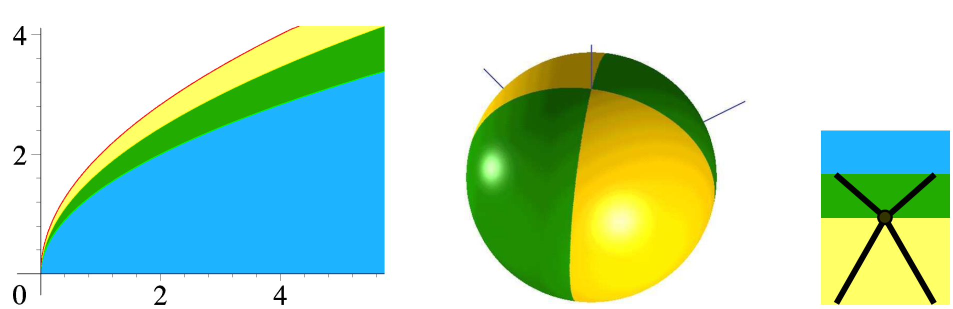

Fig. 1. (Left) Bifurcation diagram for Euler's case $\mathbf{r} = (0, 0, 0)$ with $(A_1, A_2, A_3) = (2, 1.5, 1)$. The horizontal axis is h, the vertical l. (Middle) Effective potential $U_l(\boldsymbol{\gamma})$ on the Poisson sphere, for given l. The major axes $\mathbf{e}_1$, $\mathbf{e}_2$, $\mathbf{e}_3$ point backward, upward and to the right, respectively. (Right) Reeb graph representation of the effective potential. Each point of the black graph corresponds to an equipotential line; the energy increases along the vertical. Colors indicate the topological type of $\mathcal{E}^3_{h,l}$.

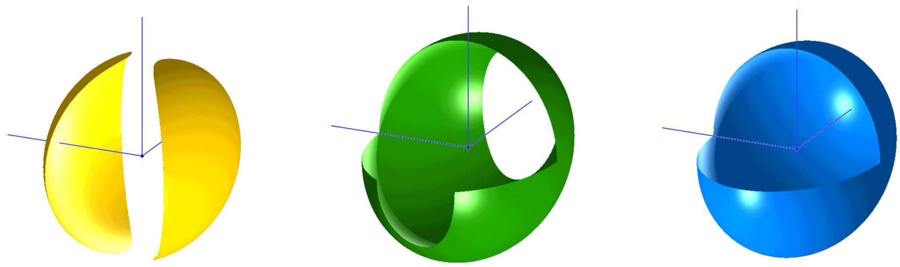

Fig. 2. Admissible angular velocities $\boldsymbol{\omega}$ for given (h, l) in the Euler case $(A_1, A_2, A_3) = (2, 1.5, 1)$. The values (h, l) are, from left to right, $(0.33, 1)$, $(0.42, 1)$, $(0.6, 1)$. In the two pictures on right, one quarter of the ellipsoid has been cut away to give a better impression of $\partial\mathcal{V}_{h,l}$.

and hence of l. $\mathcal{V}_{h,l}$ is therefore a two-dimensional set which must be contained in the ellipsoid defined by $\langle A\boldsymbol{\omega}, \boldsymbol{\omega}\rangle = 2h$. Later we shall see that if $\mathbf{r} \neq 0$, the corresponding projections $\mathcal{V}_{h,l}$ are three-dimensional sets so that it becomes meaningful to ask for their enveloping surfaces $\partial\mathcal{V}_{h,l}$. In Euler's case the issue is trivial. However, it is not trivial to ask which part of the ellipsoid is admissible to motion with given values (h, l).

A special feature of the Euler top is the extra integral $g^2 = \langle A\boldsymbol{\omega}, A\boldsymbol{\omega}\rangle$ which defines another ellipsoid in $\boldsymbol{\omega}$-space. The intersections of the two ellipsoids of constant h and g^2 are invariant lines of the $\boldsymbol{\omega}$-motion. These lines can be used to address the question of our interest: given a pair of values (h, l), which points in $\boldsymbol{\omega}$-space are then admissible? Assume first that (h, l) is taken from the yellow region in the bifurcation diagram. The smallest possible value of g^2 is obtained when the space-fixed vector $\mathbf{l}$ points in the directions of $\boldsymbol{\gamma}$ or $-\boldsymbol{\gamma}$: then $g^2 = l^2$. The invariant lines are two S^1-curves encircling the $\mathbf{e}_1$-axis in $\boldsymbol{\omega}$-space. All higher values of g^2 up to $g^2 = 2A_1h$ can be realized by adjusting the angle between $\mathbf{l}$ and $\boldsymbol{\gamma}$ such that $\langle \mathbf{l}, \boldsymbol{\gamma}\rangle$ remains equal to l. The union of the corresponding lines in $\boldsymbol{\omega}$-space is the set of two disks shown in the left part of Fig. 2. Together they are $\mathcal{V}_{h,l} = \partial\mathcal{V}_{h,l}$.

For (h, l) taken from the green region of the bifurcation diagram, the smallest possible g^2 defines two S^1-curves encircling the $\mathbf{e}_3$-direction. Again, all higher values up to $g^2 = 2A_1h$ can be realized by bending $\mathbf{l}$ sufficiently away from the direction of gravity. The resulting $\mathcal{V}_{h,l} = \partial\mathcal{V}_{h,l}$ is an annulus, see the middle part of Fig. 2.

When energy is increased into the blue region, all points on the energy ellipsoid in $\boldsymbol{\omega}$-space are admissible for an appropriate value of $g^2 > 0$, see the right part of Fig. 2.

The general invariance of $\mathbf{l}^2$ is a unique feature of the Euler case. In almost all other cases of rigid body motion in a gravitational field, the torques associated with $\mathbf{r} \neq 0$ make the angular momentum vacillate between local minima and maxima of $\mathbf{l}^2$ (for exceptions see the last sentence of Sec. 3). The admissible points in $\boldsymbol{\omega}$-space then form a three-dimensional set $\mathcal{V}_{h,l}$.

1.3. *Lagrange's case*

The Lagrange case is considerably richer in the structure of its energy surfaces and their projections to $\boldsymbol{\omega}$-space. Correspondingly, the calculations are more involved and will not be presented in this introductory chapter. We shall only illustrate the kind of results that are obtained using the methods of the subsequent sections. In line with the conventions of Sec. 5, we assume $A_2 = A_3 = \alpha A_1$ and $\mathbf{r} = \mathbf{e}_1 = (1, 0, 0)$. It has long been known [Oshemkov, 1991] that the effective potential $U_l(\boldsymbol{\gamma})$, and hence the bifurcation diagram Σ, possess different structures in the three ranges I: $1/2 < \alpha < 3/4$, II: $3/4 < \alpha < 1$, and III: $\alpha > 1$, cf. the diagonal line $\alpha = \beta$ in Fig. 13. With the procedures described in Sec. 2, it is straightforward to evaluate the critical points of the potential (6), and to obtain the three types of diagram shown in Fig. 3. Colors correspond to topological types of energy surfaces $\mathcal{E}^3_{h,l}$, their changes indicate bifurcations.

The two pictures on left in Fig. 3 represent the α-range I, corresponding to a disk-like (oblate) mass distribution. The bifurcation diagram defines four (h, l)-ranges corresponding to different topological types of energy surfaces: *one* three-sphere S^3 (red), *two* disjoint three-spheres (yellow), the projective space $\mathbb{R}P^3$ (blue), and the union of a three-sphere with the direct product $S^1 \times S^2$ (magenta). These assertions are derived from an analysis of the

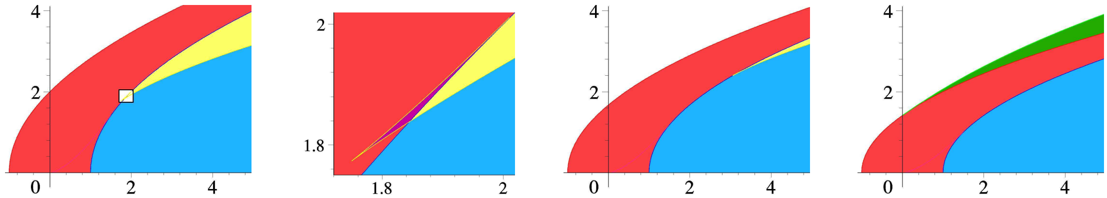

Fig. 3. Bifurcation diagrams for the three types of Lagrange tops. From left to right: $A_1 = 2$, $\alpha = 0.505$ (α-range I); a blow-up of the little window; $A_1 = 1.4$, $\alpha = 0.757$ (α-range II); $A_1 = 1$, $\alpha = 1.5$ (α-range III).

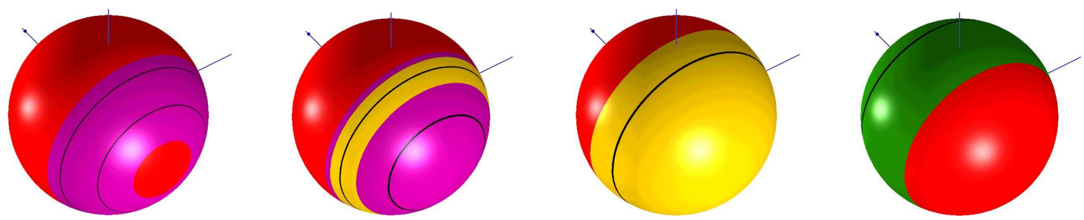

Fig. 4. Examples of Poisson spheres with contour lines of the effective potential $U_l(\boldsymbol{\gamma})$. The point $\boldsymbol{\gamma} = \mathbf{e}_1$ points backward to the upper left. The three cases on left belong to the α-range I with $\alpha = 0.505$. From left to right: $l = 1.82$ (values of the potential increase from red to magenta to red), $l = 1.85$ (red to magenta to yellow), $l = 2.1$ (red to yellow). Picture on right: $\alpha = 1.5$ (range III), $l = 3$ (green to red).

effective potential (6) of which Fig. 4 gives four examples. (The situation of low l-values is omitted there because in the color code used it would simply be represented by a red sphere.) Let us explain some details, and how the colors on the Poisson spheres are related to the colors in Fig. 3.

Notice first that the effective potential on the Poisson sphere

$$U_l(\boldsymbol{\gamma})|_{S^2} = \frac{l^2}{2A_1(\alpha + (1-\alpha)\gamma_1^2)} - \gamma_1 \qquad (10)$$

depends on γ_1 only; the equipotential lines are circles $\gamma_1 = \text{const.}$ on the Poisson sphere. A schematic view of their organization is given in Fig. 5: each point of the black Reeb graph represents an equipotential circle, the value of U_l increasing in the vertical direction. White dots correspond to $\boldsymbol{\gamma} = \mathbf{e}_1$, i.e. to "sleeping tops" in hanging position, $U_l = l^2/2A_1 - 1$. Black dots represent $\boldsymbol{\gamma} = -\mathbf{e}_1$, i.e. "sleeping tops" in upright position, $U_l = l^2/2A_1 + 1$; they may be absolute maxima, relative maxima, or even relative minima.

The color of a point $\boldsymbol{\gamma}$ on the Poisson sphere indicates the topological type of the energy surface $\mathcal{E}^3_{h,l}$ for $h = U_l(\boldsymbol{\gamma})$. Let us discuss the different color regimes. When h is larger than the absolute maximum of $U_l(\boldsymbol{\gamma})$, at given l, the corresponding $\mathcal{E}^3_{h,l}$ projects to the entire sphere S^2; its topological type is $\mathbb{R}P^3$, and the color is blue. Given a red point (h, l) in the bifurcation diagram, the projection $\mathcal{U}_{h,l}$ of $\mathcal{E}^3_{h,l}$ is a disk $D^2 \sim S^2\backslash D^2$ on the $\boldsymbol{\gamma}$-sphere which is bounded by an equipotential line in the red region; the corresponding type of $\mathcal{E}^3_{h,l}$ is S^3. For sufficiently low values of l^2, only the red and blue types of energy surfaces occur; cf. the left picture in Fig. 5.

For l-values in a small range around 1.8, see the blow-up in Fig. 3, the potential $U_l(\boldsymbol{\gamma})$ has a degenerate relative minimum ($h = 1.807$ for $l = 1.82$) along the right black circle in the magenta region of the leftmost picture in Fig. 4. With these values of h and l, the Lagrange top is in a stable relative equilibrium, rotating at a fixed inclination with respect to the direction of gravity. With slightly higher values of h, there exists, in addition to the disk with center at $\boldsymbol{\gamma} = \mathbf{e}_1$, an annulus $S^2\backslash 2D^2$ of accessible $\boldsymbol{\gamma}$-values around that circle; hence the energy surface has two disjoint components: a three-sphere and a direct product $S^1 \times S^2$ (magenta). As energy increases towards $h = 1.81825$, a degenerate relative maximum along the left black $\boldsymbol{\gamma}$-circle is reached. The annulus merges with the disk, forming a larger disk, and the energy surface becomes again a single three-sphere (red). The absolute maximum of $U_l(\boldsymbol{\gamma})$ is located at $\boldsymbol{\gamma} = -\mathbf{e}_1$ (upright sleeping top). The second picture from left in Fig. 5 shows how the equipotential lines are connected.

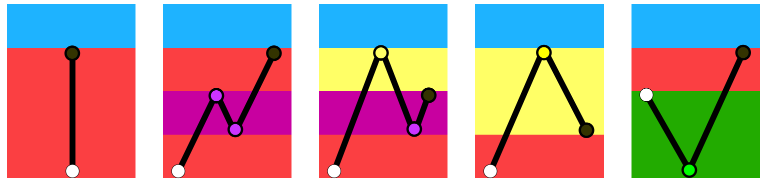

Fig. 5. Reeb graphs for effective potentials in the α-range I with (from left to right) $l = 0$, $l = 1.82$, $l = 1.85$, $l = 2.1$, and α-range III with $l = 3$ (right). The white dots correspond to sleeping tops in hanging position $\boldsymbol{\gamma} = \mathbf{e}_1$, black dots to sleeping tops in upright position $\boldsymbol{\gamma} = -\mathbf{e}_1$; colored dots indicate critical circles.

Next consider $l = 1.85$. Again, there exists a critical circle, with a relative minimum of U_l, in the magenta region, and an annulus of accessible $\boldsymbol{\gamma}$-values for h slightly higher. But before this annulus has a chance to merge with the disk, its hole at $\boldsymbol{\gamma} = -\mathbf{e}_1$ closes (relative maximum at the upright sleeping position) so that $\mathcal{E}^3_{h,l}$ consists of two disjoint three-spheres (yellow). The transition to $\mathbb{R}P^3$ (blue) is now via the critical circle in the center of the yellow region of the Poisson sphere.

The last possibility in the α-range I is illustrated in the second images from right in Figs. 4 and 5. At sufficiently high l^2, the upright sleeping top $\boldsymbol{\gamma} = -\mathbf{e}_1$ is a relative minimum of U_l, corresponding to a stable motion. The absolute maximum is assumed along a critical circle. Hence the sequence of accessible regions on the Poisson sphere, as h increases, is D^2, $2D^2$, S^2, corresponding to energy surfaces S^3, $2S^3$, $\mathbb{R}P^3$.

Figure 3 shows that the α-range II is simpler than I: the effective potential has only red and yellow regions, and there are no new types of behavior. However, range III, corresponding to cigar shaped (prolate) mass distributions, exhibits a new kind of motion (green color). At sufficiently high values of l^2, the effective potential assumes its absolute minimum not in $\mathbf{e}_1$ but along a circle of constant γ_1, corresponding to a kind of merry-go-round motion. The accessible $\boldsymbol{\gamma}$-region at low energy is therefore an annulus, the energy surface of topological type $S^1 \times S^2$.

The main question addressed in this paper concerns the projections $\mathcal{V}_{h,l}$ of the energy surfaces $\mathcal{E}^3_{h,l}$ to the space $\mathbb{R}^3(\boldsymbol{\omega})$ of angular velocities. More precisely, we are concerned with the topological nature of their envelopes $\partial\mathcal{V}_{h,l}$; these are the projections to $\boldsymbol{\omega}$-space of the submanifolds $\mathcal{P}^2_{h,l}$ of $\mathcal{E}^3_{h,l}$ where $\mathbf{l}^2$ assumes an extremal value. We shall see that, in general, the topology of $\mathcal{P}^2_{h,l}$ and $\partial\mathcal{V}_{h,l}$ depends not only on the topology of $\mathcal{E}^3_{h,l}$ but also on details discussed in Secs. 4 and 6. For the Lagrange case, it turns out that all manifolds $\mathcal{P}^2_{h,l}$ are two-tori: single T^2 in the red, blue and green regions, pairs of T^2 in the yellow and magenta regions. The projection of $\mathcal{P}^2_{h,l}$ to $\boldsymbol{\omega}$-space possesses, in general, up to three singular points on the axis where $\mathbf{l} = A\boldsymbol{\omega}$ is collinear with $\mathbf{r}$. For the Lagrange case this means there may be up to three singular points on the $\mathbf{e}_1$-axis, see Fig. 7. Their number is 0 in the green region of the bifurcation diagram, 1 for both components of $\partial\mathcal{V}_{h,l}$ in the yellow region, 2 in the blue region, 1 and 0 for the components related to S^3 and $S^1 \times S^2$ in the magenta region.

The red region deserves special attention. It is separated in two parts by the line $h^3 = 27l^2/8A_1$, $0 \le h \le 3/2$, see Eq. (49) and Fig. 6 where the bifurcation sets Σ are shown for the same parameters as in Fig. 3, together with the extra line (color

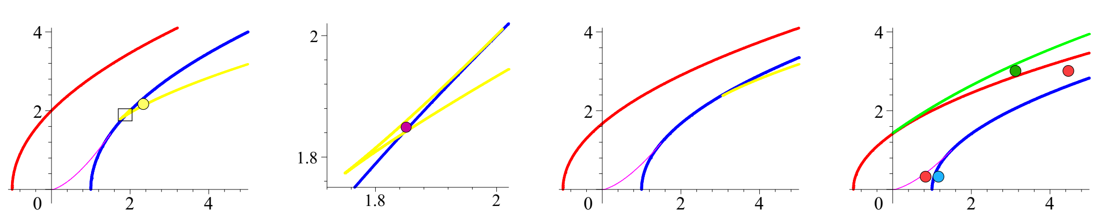

Fig. 6. Bifurcation sets Σ for the same parameters as in Fig. 3, plus the extra bifurcation line (49) for the surfaces $\partial\mathcal{V}_{h,l}$ (magenta). The fat colored dots indicate the (h, l) values for which the six surfaces in Fig. 7 are drawn.

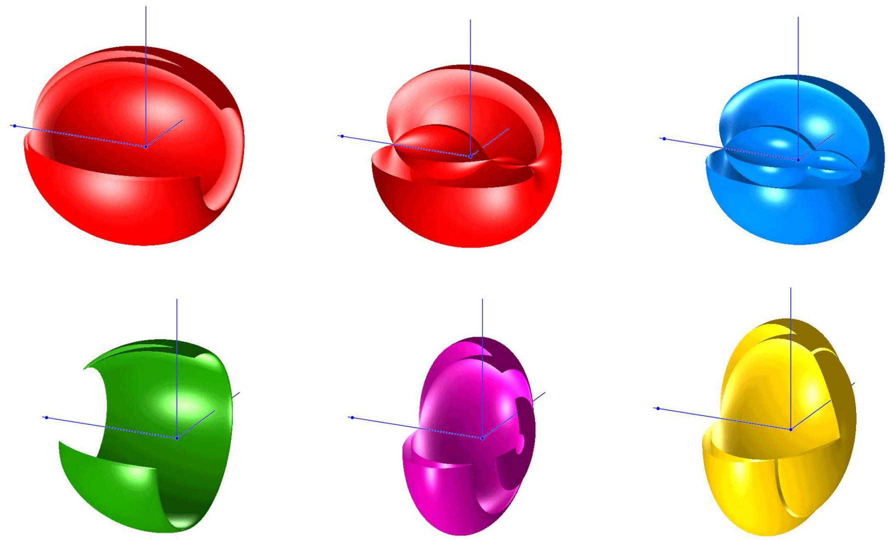

Fig. 7. The six kinds of enveloping surfaces $\partial\mathcal{V}_{h,l}$ in $\boldsymbol{\omega}$-space, for Lagrange tops. The two red surfaces as well as the blue and green are computed for $A_1 = 1$, $\alpha = 1.5$ (α-range III), the magenta and yellow surfaces for $A_1 = 2$, $\alpha = 0.505$ (α-range I). In the upper row, the values (h, l) are (4.5, 3), (0.85, 0.3), (1.1, 0.3); in the lower row they are (3.1, 3), (1.851, 1.85), (2.307, 2.1). The direction $\boldsymbol{\omega} = \mathbf{e}_1$ points to the left. All surfaces possess rotational symmetry with respect to $\mathbf{e}_1$; one quarter has been cut away to make the inside visible.

magenta). This line is not related to singularities of $\mathcal{E}^3_{h,l}$ or $\mathcal{P}^2_{h,l}$; rather it reflects a singularity of the projection. For values (h, l) in the red region to the left or above the line, the surfaces $\partial\mathcal{V}_{h,l}$ have one singular point; for (h, l) to right and below the line, they have three, cf. the two red pictures in Fig. 7.

The envelopes enclose the regions of admissible angular velocities. Trajectories $\boldsymbol{\omega}(t)$ remain in $\mathcal{V}_{h,l}$ and are tangent to $\partial\mathcal{V}_{h,l}$, where $d\mathbf{l}^2/dt = 0$. The outer part of the envelopes corresponds to local maxima of $\mathbf{l}^2$, the inner part to local minima. The extra constant of motion $l_s = \langle \mathbf{l}, \mathbf{r} \rangle$ of the Lagrange case implies that the trajectories are restricted to planes $\omega_1 = l_s/A_1$. The intersections of these planes with $\partial\mathcal{V}_{h,l}$ are the invariant foliation of $\partial\mathcal{V}_{h,l}$ by projections of Liouville–Arnold tori from the reduced phase space to $\boldsymbol{\omega}$-space.

1.4. *General case: Outline of the paper*

The focus of mathematical research in rigid body dynamics has always been on the integrable cases. In recent years, considerable progress has been made in the development of analytic and geometric methods of their investigation. Fomenko's scientific school (see [Bolsinov & Fomenko, 1999] for a review) has developed a "molecular" theory of topological classification of integrable systems which allows us to describe and compare dynamical systems in great detail. To take the most prominent example: a deep understanding of the Kovalevskaya system in all its complexity has only recently been achieved. In her original work, Kovalevskaya [Kowlevski, 1890] proved its integrability and showed that it could be solved in terms of theta functions; Kötter [1893] pursued that kind of analysis in greater detail. More qualitative analytic investigations were initiated by Zhukovskii [Zhukovskii, 1896; Appelrot, 1940], but a full description of the bifurcation diagram was only given by Iacob [1971] and Kharlamov [1988]. On that basis, the action variables could be determined [Dullin, 1994; Dullin *et al.*, 1994; Dullin *et al.*, 1998], and the Liouville foliations were described in all detail [Bolsinov *et al.*, 2000]. The dynamics of the body in time could be formulated, on a basic level, in terms of Lax pairs [Bobenko *et al.*, 1989], and a detailed description in primary Euler–Poisson variables was given in [Gashenenko, 2000]. For a survey on the present state of affairs, we recommend the Conference Proceedings [Kuznetzov & Nijhoff, 2000]. Klein and Sommerfeld [1910] had already discussed the idea of attacking the more general non-integrable systems by interpolation of solutions for the integrable cases. But in spite of all modern advancement, this is still hope rather than practice.

The present paper is an attempt to use ideas from the theory of integrable systems and provide a basis for the study of arbitrary rigid body systems. This is done in the spirit of the topological research program that was initiated by Smale [1970]. The program is based on Morse theory [Milnor, 1963] and, when applied to the Euler–Poisson Eqs. (1), suggests to first study the topology and bifurcations of $\mathcal{E}^3_{h,l}$, and then to look for further invariant sets on each separate energy surface (see also [Abraham & Marsden, 1978; Lewis *et al.*, 1992]). We refer to [Smale, 1970; Tatarinov, 1973; McCord *et al.*, 1998; Bolsinov & Fomenko, 1999] as successful examples where the program was applied to diverse classical systems. Applications of Smale's constructive theory to rigid body dynamics were developed in [Iacob, 1971; Katok, 1972; Tatarinov, 1974; Oshemkov, 1991]. Our contribution with this paper is the analysis of the topology and the bifurcation scheme of the enveloping surfaces $\partial\mathcal{V}_{h,l}$ of the natural projections $\mathcal{V}_{h,l}$ of $\mathcal{E}^3_{h,l} \subset \mathbb{R}^3(\boldsymbol{\omega}) \times S^2(\boldsymbol{\gamma})$ to the space $\mathbb{R}^3(\boldsymbol{\omega})$ of angular velocities. These surfaces are the loci of local extrema in the modulus of the angular momenta $|A\boldsymbol{\omega}|$. Their pre-images $\mathcal{P}^2_{h,l}$ in $\mathcal{E}^3_{h,l}$ are two-dimensional manifolds which we recommend as perhaps the best general choice for complete Poincaré surfaces of section [Dullin & Wittek, 1995]. An application of this idea to the integrable Kovalevskaya case was given earlier in [Gashenenko, 2000]. In the following, we extend it to the general case of Eqs. (1), and give a number of examples for illustration.

The paper is organized as follows. Section 2 recalls the construction in $(h,\, l)$-space of bifurcation diagrams Σ of the energy surfaces $\mathcal{E}^3_{h,l}$. The well-known method is based on a study of the projections $\mathcal{U}_{h,l}$ of $\mathcal{E}^3_{h,l}$ to the Poisson sphere $S^2(\boldsymbol{\gamma})$. The essential task is to identify the relative equilibria of the Euler–Poisson equations from the properties of an effective potential. The brief Sec. 3 is a recollection of the Hess equations: the Euler–Poisson equations written in terms of the angular velocities only; the variables $\boldsymbol{\gamma}$ have been eliminated in favor of the integration constants. At this point it becomes possible to characterize the enveloping surface $\partial\mathcal{V}_{h,l}$ in $\boldsymbol{\omega}$-space as the level set $f(\boldsymbol{\omega}) = 0$ of an explicitly given function. Section 4 studies the pre-images $\mathcal{P}^2_{h,l}$ in $\mathcal{E}^3_{h,l}$ of the enveloping surfaces. It turns out that the bifurcation diagram $\tilde{\Sigma}$ of its topological types contains Σ and, in general, three additional lines in the $(h,\, l)$-plane. The main tool for the derivation of these results is the projection $\tilde{\mathcal{U}}_{h,l}$ of $\mathcal{P}^2_{h,l}$ to the Poisson sphere. We present examples where the role of the additional bifurcation lines is made clear. Before we turn to the main results, Sec. 5 gives a complete survey of the bifurcation diagrams, for $\mathcal{E}^3_{h,l}$ and $\mathcal{P}^2_{h,l}$, in the two-parameter family of rigid bodies studied by Katok [1972]. The family is special in that $\tilde{\Sigma}$ and Σ are identical, but still it is rich enough to exhibit ten different types of enveloping surfaces $\partial\mathcal{V}_{h,l}$. These surfaces are studied in the last Sec. 6. Their bifurcation scheme is even richer than that of $\mathcal{P}^2_{h,l}$, as the projection to $\boldsymbol{\omega}$-space tends to introduce up to three singular points. These are the only possible vectors $\boldsymbol{\omega}$ on the line where the angular momentum $A\boldsymbol{\omega}$ is collinear with $\mathbf{r}$.

2. Bifurcation Sets of Energy Surfaces $\mathcal{E}^3_{h,l}$

The topological type of an energy surface $\mathcal{E}^3_{h,l}$ is uniquely determined by its projection $\mathcal{U}_{h,l} = \pi(\mathcal{E}^3_{h,l})$ on the Poisson sphere $S^2(\boldsymbol{\gamma}) = \{|\boldsymbol{\gamma}| = 1\}$, where $\pi : (\boldsymbol{\omega},\, \boldsymbol{\gamma}) \mapsto \boldsymbol{\gamma}$. The compact set $\mathcal{U}_{h,l} \subset S^2$, called *the domain of possible configurations*, consists of those points of the unit sphere for which $U_l \leq h$, where U_l is the *effective potential* defined in (6). The manifold $\mathcal{E}^3_{h,l}$ is diffeomorphic to a fiber bundle with the base $\mathcal{U}_{h,l}$ and fibers S^1, where fibers over $\partial\mathcal{U}_{h,l}$ are identified as points. When $\partial\mathcal{U}_{h,l}$ contains a critical point of U_l, the set $\mathcal{E}^3_{h,l}$ is not a manifold but a separatrix where the topology of these manifolds changes. The corresponding pair $(h,\, l)$ belongs to the bifurcation set $\Sigma \subset \mathbb{R}^2(h,\, l)$ of the momentum map $\mathcal{F}$.

In order to find the bifurcation set Σ we use the fact [Tatarinov, 1973] that the critical points of the effective potential U_l are in one-to-one correspondence with the relative equilibria, or steady rotations about the vertical axis. That is, we identify all critical points corresponding to the relative equilibria, and insert them into the integrals (2) to obtain all critical values of the momentum map $\mathcal{F}$. From a long list of available literature we refer here only to the three classical treatises [Ampère, 1821; Routh, 1884; Staude, 1894], where the steady rotations of a rigid body were studied under the most general assumptions.

Without loss of generality, let the moments of inertia be ordered according to $A_1 \geq A_2 \geq A_3$, and let the r_i be non-negative. In the nondegenerate case $r_1r_2r_3 \neq 0$, a parametric representation of the bifurcation set may be obtained as follows. First, conclude from $\dot{\boldsymbol{\gamma}} = 0$ that $\boldsymbol{\omega} = \mu\boldsymbol{\gamma}$ with $\mu \in \mathbb{R}$.

Next, solve the equations $\dot{\boldsymbol{\omega}} = 0$ with the ansatz $\gamma_i(A_i - \sigma) = r_i/\mu^2$, where

$$\sigma \in (-\infty,\, A_3) \cup (A_3,\, A_2) \cup (A_2,\, A_1) \cup (A_1,\, \infty)\,. \tag{11}$$

The geometric integral $\langle \boldsymbol{\gamma}, \boldsymbol{\gamma} \rangle = 1$ then leads to

$$\mu = \left(\frac{r_1^2}{(A_1 - \sigma)^2} + \frac{r_2^2}{(A_2 - \sigma)^2} + \frac{r_3^2}{(A_3 - \sigma)^2} \right)^{\frac{1}{4}}. \tag{12}$$

In the last step, insert these expressions in the energy and angular momentum integrals to obtain Σ as parameterized by σ:

$$h = \frac{1}{\mu^2} \left(\frac{\left(\frac{3}{2} A_1 - \sigma\right) r_1^2}{(A_1 - \sigma)^2} + \frac{\left(\frac{3}{2} A_2 - \sigma\right) r_2^2}{(A_2 - \sigma)^2} + \frac{\left(\frac{3}{2} A_3 - \sigma\right) r_3^2}{(A_3 - \sigma)^2} \right),$$

$$l = \frac{1}{\mu^3} \left(\frac{A_1 r_1^2}{(A_1 - \sigma)^2} + \frac{A_2 r_2^2}{(A_2 - \sigma)^2} + \frac{A_3 r_3^2}{(A_3 - \sigma)^2} \right). \tag{13}$$

For each of the two signs of μ, corresponding to the signs of l, we obtain four connected pieces of Σ. The left picture in Fig. 8 shows an example. The piece $\sigma \in (A_1, \infty)$ (red) gives the highest physically possible l^2 at given h, or the lowest possible energy at given l^2; conversely, the piece $\sigma \in (-\infty, A_3)$ (blue) gives the relative equilibria with highest possible h at given l^2. For $\sigma \to \pm\infty$, the limiting points are the two absolute equilibria $(h, l) = (\mp|\mathbf{r}|, 0)$, and for $\sigma = A_i + \epsilon$ with $\epsilon \to 0$, the curves behave as $h \approx l^2/(2A_i) - r_i \,\mathrm{sgn}(\epsilon)$. When $A_1 = A_2$ or $A_2 = A_3$, one of the pieces disappears, and when all three A_i are equal, Σ contains only two parts.

If the body's center of gravity lies on one of the principal planes of inertia, then (13) gives only three of the four pieces of the bifurcation set (for each sign of μ, or l). For example, if $r_3 = 0$, we must distinguish the two possibilities $\gamma_3 = 0$ and $\gamma_3 \neq 0$. In the former case, the expressions (12) and (13), without the last terms, are still valid, but σ runs through only three intervals $(-\infty, A_2) \cup (A_2, A_1) \cup (A_1, \infty)$. It is then convenient to introduce the parameter τ via $\sigma = (A_1 r_2 + A_2 r_1 \tau)/(r_2 + r_1 \tau)$, and to eliminate μ:

$$h = (A_2 r_1 \tau^3 + (3A_2 - 2A_1) r_2 \tau^2 + (3A_1 - 2A_2) r_1 \tau + A_1 r_2)/(2(A_1 - A_2)|\tau|\sqrt{1 + \tau^2}),$$

$$l = \frac{|r_2 + r_1 \tau|^{1/2}}{|\tau|^{1/2}(1 + \tau^2)^{3/4}} \frac{A_1 + A_2 \tau^2}{(A_1 - A_2)^{1/2}}. \tag{14}$$

where $\tau \in (-\infty, -r_2/r_1) \cup (-r_2/r_1, 0) \cup (0, \infty)$. The sign of the square root in the equation for h must be taken as $\mathrm{sgn}((r_2/r_1) - \tau)$. The fourth piece of Σ is obtained with $\gamma_3 \neq 0$, and again $\boldsymbol{\omega} = \mu \boldsymbol{\gamma}$ but $\gamma_i(A_i - A_3) = r_i/\mu^2$. The normalization $\langle \boldsymbol{\gamma}, \boldsymbol{\gamma} \rangle = 1$ implies

$$\omega_3^2 = \mu^2 - \mu_0^4/\mu^2$$

with $$\mu_0^4 = \frac{r_1^2}{(A_1 - A_3)^2} + \frac{r_2^2}{(A_2 - A_3)^2} \tag{15}$$

Using μ as a parameter in the intervals $|\mu| \in (\mu_0, \infty)$, the corresponding pieces of Σ are given by

$$h = \frac{1}{2} A_3 \mu^2 + \frac{3}{2} \frac{\alpha}{\mu^2}, \qquad l = A_3 \mu + \frac{\alpha}{\mu^3}, \tag{16}$$

with

$$\alpha = \frac{r_1^2}{A_1 - A_3} + \frac{r_2^2}{A_2 - A_3}.$$

Similar representations of Σ hold for $r_1 = 0$ or $r_2 = 0$. An example is shown in the middle image of Fig. 8. The red, blue and yellow branches of Σ are given by (14) while the green piece comes from (16).

Finally, if the center of mass falls on one of the principal axes of inertia, (13) gives only two pieces of Σ (for each sign of μ, or l). For example, if $r_2 = r_3 = 0$, we must distinguish three cases. The first, $\gamma_2 = \gamma_3 = 0$, is described by (12) and (13) with only their first terms, and $\sigma \in (-\infty, A_1) \cup (A_1, \infty)$. It is straightforward to see that this leads to the two curves

$$h = \frac{l^2}{2A_1} \pm r_1\,. \tag{17}$$

The second case is $\gamma_3 = 0$, $\gamma_2 \neq 0$, and gives the line

$$h = \frac{1}{2} A_i \mu^2 + \frac{3}{2} \frac{\alpha_i}{\mu^2}, \qquad l = A_i \mu + \frac{\alpha_i}{\mu^3}, \tag{18}$$

with

$$\alpha_i = \frac{r_1^2}{A_1 - A_i} \quad \text{and} \quad \mu^2 > \frac{\alpha_i}{r_1}$$

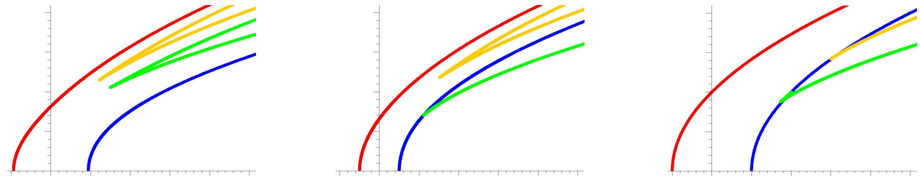

Fig. 8. Bifurcation diagrams with $A_1 = 2$, $A_2 = 1.5$, $A_3 = 1$ and $(r_1, r_2, r_3) = (0.3, 0.4, 0.8)$ (left), $(0.3, 0.4, 0)$ (middle), $(1, 0, 0)$ (right). The horizontal axis is h, the vertical l; the major tick marks are separated by unity.

and $i = 2$. The last piece of Σ is obtained with $\gamma_2 = 0$, $\gamma_3 \neq 0$ and is again described by (18) with $i = 3$. The right image in Fig. 8 gives an example. The red and blue branches correspond to (17), the yellow and green pieces to (18) with $i = 2$ and $i = 3$, respectively.

The structure of such bifurcation diagrams Σ was investigated in [Iacob, 1971; Katok, 1972; Tatarinov, 1974]. However, an exhaustive study of the full space of parameters $\{A_1, A_2, A_3, r_1, r_2, r_3\}$ (which may be reduced to four dimensions by appropriate scaling such as $|\mathbf{r}| = 1$ and $\det A = 1$) has not yet been presented. A complete analysis of the two-dimensional subspace $r_2 = r_3 = 0$ was given by Katok [1972] and will be reviewed in Sec. 5.

Each diagram divides the plane $\mathbb{R}^2(h, l)$ into connected domains, or *zones*, inside which the topological type of $\mathcal{E}^3_{h,l}$ is preserved. Morse theory [Milnor, 1963] can be used to establish this type for every zone of $\mathbb{R}^2(h, l)\backslash\Sigma$. Tatarinov [1974], in an attempt to extend Katok's results, investigated various special and general cases for the parameters A_i, r_i. He found that connected components of nonsingular energy surfaces $\mathcal{E}^3_{h,l}$ are diffeomorphic to one of the following manifolds: the sphere S^3, the product space $S^1 \times S^2$, the real projective space $\mathbb{R}P^3$, or the connected sum $(S^1 \times S^2)\#(S^1 \times S^2)$. (The latter manifold has been given different names by different authors. In [Bolsinov & Fomenko, 1999] it is designated as K^3. Arnold [1974] calls it a "*pretzel*" *obtained from the three-sphere* S^3 *by attaching two* "*handles*" *of the form* $S^1 \times D^2$.) The corresponding connected components of their projections $\mathcal{U}_{h,l} = \pi(\mathcal{E}^3_{h,l})$ on the Poisson sphere are a disk D^2, an annulus $D^2\backslash D^2$, a disk with two holes $D^2\backslash 2D^2$, or the full sphere S^2 [Bolsinov *et al.*, 1996]. All these cases already occur in Katok's special case $r_2 = r_3 = 0$. It appears that the following conjecture is true: there exist no more than ten isolated critical points of the effective potential on the Poisson sphere; the above list of four types of nonsingular energy surfaces $\mathcal{E}^3_{h,l}$ is complete; any $\mathcal{E}^3_{h,l}$ consists of no more than three connected components.

As an illustration, for the three parameter sets of Fig. 8, consider the three rows of Fig. 9. Each picture shows level sets of the effective potential U_l. The two equilibrium positions (for $l = 0$) are indicated as thick dots, the north pole $\boldsymbol{\gamma} = \mathbf{r}/|\mathbf{r}| =: \hat{\mathbf{r}}$ near the top or the right boundary in blue (stable equilibrium), the south pole $\boldsymbol{\gamma} = -\hat{\mathbf{r}}$ near the bottom or the center in brown (unstable equilibrium). Let us explain a few features.

The first row corresponds to the left picture in Fig. 8, with three values of l. With $l = 1$ (left), the potential has a minimum near the north pole, a maximum near the south pole, and no further critical point. Hence $\mathcal{U}_{h,l}$ is either a disk or the full sphere, the energy surface either S^3 or $\mathbb{R}P^3$. For l-values slightly above the tip of the green line of relative equilibria, the picture in the middle shows that a saddle-node bifurcation has occurred; for energies between the level of the saddle and the local maximum, $\mathcal{U}_{h,l}$ is an annulus and $\mathcal{E}^3_{h,l}$ the product manifold $S^1 \times S^2$. The yellow line of relative equilibria Fig. 8 introduces another saddle-node pair, as can be seen in the picture at right. However, the saddle has now the higher level; hence, in the energy range enclosed by the yellow line, $\mathcal{U}_{h,l}$ consists of two disks, the energy surface of two S^3.

The second row is for $\mathbf{r} = (0.3, 0.4, 0)$. The sequence of changes, as l increases, is similar as in the first row. The difference is the symmetry with respect to $\gamma_3 \to -\gamma_3$, and the fact that the two holes of the $\mathcal{U}_{h,l}$-annulus close simultaneously, at the green relative equilibrium line.

The third row shows the case $\mathbf{r} = (1, 0, 0)$ which possesses two symmetries. There is a small range of l-values, near the cusp of the green line, where the potential allows $\mathcal{U}_{h,l}$ to be a disk with two holes; the energy surface is then of type $(S^1 \times S^2)\#(S^1 \times S^2)$ (second image from left). At higher values of l (second image from right), the maximum

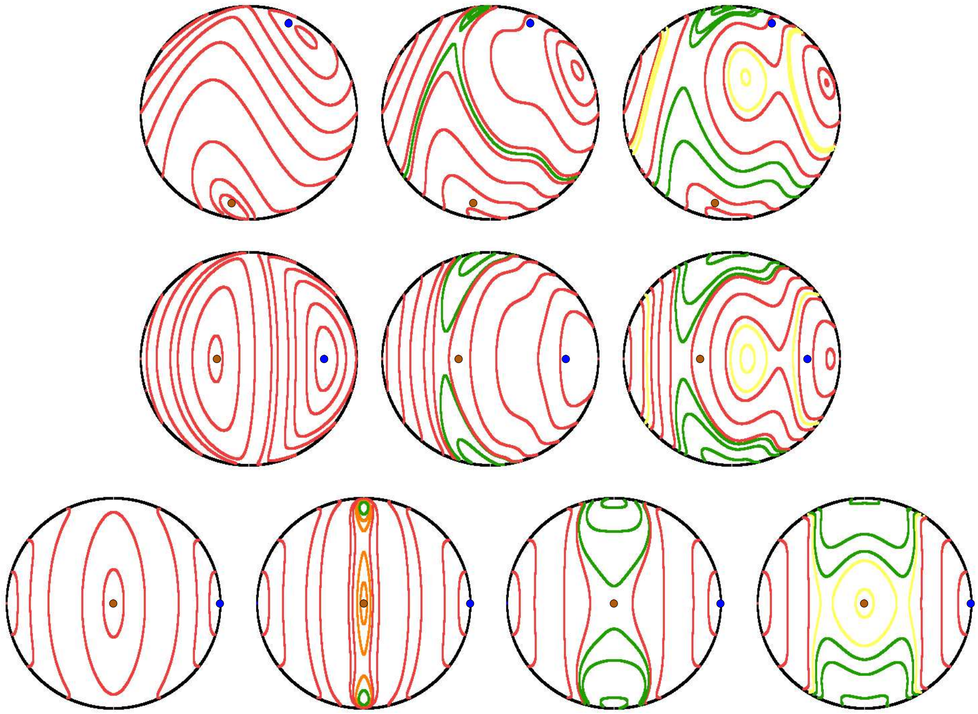

Fig. 9. Level sets of the potential U_l for the parameters of Fig. 8. The right boundary of this projection of the entire Poisson sphere is to be identified with the left boundary. Upper row: $\mathbf{r} = (0.3,\, 0.4,\, 0.8)$; left: $l = 1$, middle: $l = 2.29$, right: $l = 3$. Second row: $\mathbf{r} = (0.3,\, 0.4,\, 0)$; left: $l = 0.5$, middle: $l = 2$, right: $l = 3$. Third row: $\mathbf{r} = (1,\, 0,\, 0)$; from left to right: $l = 1$, $l = 1.85$, $l = 2.5$ $l = 3.5$.

at the south pole turns into a saddle point, and the only possibilities for $\mathcal{U}_{h,l}$ are disk, annulus, full sphere. Finally, when the yellow relative equilibrium line appears, the south pole becomes a relative minimum, and the sequence for $\mathcal{U}_{h,l}$, as energy increases, is disk, two disks, annulus, full sphere.

3. Hess Equations and Enveloping Surface

The traditional use of projections $\mathcal{U}_{h,l} = \pi(\mathcal{E}^3_{h,l}) \subset S^2(\boldsymbol{\gamma})$ for a classification of the energy surfaces naturally suggests the question on how the corresponding projections $\mathcal{V}_{h,l} = p(\mathcal{E}^3_{h,l}) \subset \mathbb{R}^3(\boldsymbol{\omega})$ look like, where $p : (\boldsymbol{\omega},\, \boldsymbol{\gamma}) \mapsto \boldsymbol{\omega}$ projects to the body-fixed space of angular velocities. From a physical point of view the angular velocity $\boldsymbol{\omega}$ contains more important information about the motion than the unit vector $\boldsymbol{\gamma}$ of the direction of gravity. In this connection it may suffice to recall Poinsot's geometric interpretation of the motion in terms of a body-fixed axoid carrying the locus of angular velocities (the polhode) rolling along a surface which carries the corresponding locus in inertial space (the herpolhode); the point of contact determines the angular velocity both in the space-fixed and the body-fixed system [Whittaker, 1964; Arnold, 1974].

To find the projection $\mathcal{V}_{h,l}$ we must express the Euler–Poisson equations on a given integral surface $\mathcal{E}^3_{h,l}$ in terms of $\boldsymbol{\omega}$ only. This was in fact done by Hess [Hess, 1890; Golubev, 1953] who eliminated $\boldsymbol{\gamma}$ from the system (1) with the help of the integrals (2) and derived several new versions of the dynamical equations. One form of these equations is particularly useful for our purposes. Suppose that the vectors $A\boldsymbol{\omega}$ and $\mathbf{r}$ are not collinear for all times, and decompose the vector $\boldsymbol{\gamma}$ in the following way:

$$\boldsymbol{\gamma} = \zeta_1 A\boldsymbol{\omega} + \zeta_2 \mathbf{r} + \zeta_3 A\boldsymbol{\omega} \times \mathbf{r}\,. \tag{19}$$

Using the integrals H, L, I, we find the coefficients

$$\begin{aligned}
\zeta_1 &= \frac{|\mathbf{r}|^2 l - (T-h)\langle A\boldsymbol{\omega},\, \mathbf{r}\rangle}{|A\boldsymbol{\omega} \times \mathbf{r}|^2}\,, \\
\zeta_2 &= \frac{(T-h)|A\boldsymbol{\omega}|^2 - \langle A\boldsymbol{\omega},\, \mathbf{r}\rangle l}{|A\boldsymbol{\omega} \times \mathbf{r}|^2}\,, \\
\zeta_3 &= \frac{\sqrt{f}}{|A\boldsymbol{\omega} \times \mathbf{r}|^2}
\end{aligned} \tag{20}$$

where

$$T = \frac{1}{2}\langle A\boldsymbol{\omega}, \boldsymbol{\omega}\rangle ,$$
$$f = |A\boldsymbol{\omega} \times \mathbf{r}|^2 - |(T-h)A\boldsymbol{\omega} - l\mathbf{r}|^2 . \tag{21}$$

Elementary transformations allow us to write $f(\boldsymbol{\omega})$ as a polynomial of the sixth order in the three variables ω_i:

$$\begin{aligned} f &= (|A\boldsymbol{\omega}|^2 - l^2)(|\mathbf{r}|^2 - (T-h)^2) \\ &\quad - [\langle A\boldsymbol{\omega}, \mathbf{r}\rangle - (T-h)l]^2 \\ &= -T^2|A\boldsymbol{\omega}|^2 + 2hT|A\boldsymbol{\omega}|^2 + 2lT\langle A\boldsymbol{\omega}, \mathbf{r}\rangle \\ &\quad + |A\boldsymbol{\omega}|^2(|\mathbf{r}|^2 - h^2) - \langle A\boldsymbol{\omega}, \mathbf{r}\rangle^2 \\ &\quad - 2hl\langle A\boldsymbol{\omega}, \mathbf{r}\rangle - l^2|\mathbf{r}|^2 . \end{aligned} \tag{22}$$

Substituting (19) in the first equation of (1), we obtain the vector form of the Hess equations:

$$A\dot{\boldsymbol{\omega}} = A\boldsymbol{\omega} \times \boldsymbol{\omega} + \zeta_1 \mathbf{r} \times A\boldsymbol{\omega} + \zeta_3 \mathbf{r} \times (A\boldsymbol{\omega} \times \mathbf{r}) . \tag{23}$$

The equation does not contain $\boldsymbol{\gamma}$. It describes the dynamics of the angular velocity $\boldsymbol{\omega}$ and the angular momentum $A\boldsymbol{\omega}$ in a body-fixed basis. Kharlamov proved [1965] that the function $f(\boldsymbol{\omega})^{-\frac{1}{2}}$ serves as an *integrating factor* for Eq. (23), hence one additional integral without explicit time dependence, if it exists, suffices to reduce (23) to quadratures [Golubev, 1953]. In any case, the solution of (23) together with (19) can be used to reduce the φ-Eq. (5) to a quadrature without involving the γ's.

The function $f(\boldsymbol{\omega})$ is closely connected to the projection $\mathcal{V}_{h,l} = p(\mathcal{E}^3_{h,l})$ of the energy surface to the space $\mathbb{R}^3(\boldsymbol{\omega})$ of angular velocities. Namely, a point $\boldsymbol{\omega}$ belongs to $\mathcal{V}_{h,l}$ if and only if there exists a real set $(\gamma_1, \gamma_2, \gamma_3)$, satisfying the three first integrals. The boundary of this set is given by the condition

$$\frac{D(H, L, I)}{D(\gamma_1, \gamma_2, \gamma_3)} = 0 \tag{24}$$

which leads to the equality

$$F := \langle \mathbf{r}, A\boldsymbol{\omega} \times \boldsymbol{\gamma}\rangle = 0 . \tag{25}$$

Now we may use the Hess method to eliminate $\boldsymbol{\gamma}$ and find that $F = 0$ reduces to $f(\boldsymbol{\omega}) = 0$ in the space $\mathbb{R}^3(\boldsymbol{\omega})$. Thus the domain of accessible velocities $\mathcal{V}_{h,l}$ is bounded by the closed two-dimensional set

$$\partial\mathcal{V}_{h,l} = \{f(\boldsymbol{\omega}) = 0\} \subset \mathbb{R}^3(\boldsymbol{\omega}) \tag{26}$$

which we call the *enveloping surface*. The projections of the phase space trajectories corresponding to fixed values (h, l) fill in the closed domain $\mathcal{V}_{h,l} = \{f(\boldsymbol{\omega}) \geq 0\} \subset \mathbb{R}^3(\boldsymbol{\omega})$. It follows from the equality (19) that each interior point of the set $\mathcal{V}_{h,l}$ has two and only two pre-images on the surface $\mathcal{E}^3_{h,l}$. They differ by the sign of the coefficient ζ_3.

Note that the equality

$$\frac{1}{2}\frac{d}{dt}|A\boldsymbol{\omega}|^2 = \sqrt{f(\boldsymbol{\omega})} , \tag{27}$$

follows directly from (23); it is known as one of Hess' equations. Any trajectory — also called *hodograph* — of the angular velocity in the set $\mathcal{V}_{h,l}$ becomes a tangent to the enveloping surface $\partial\mathcal{V}_{h,l}$ when $|A\boldsymbol{\omega}|$ assumes a local extremum. If the trajectory belongs entirely to the surface $\partial\mathcal{V}_{h,l}$, then, in accordance with (27), the modulus of the angular momentum preserves its initial value. It is known that there are just four cases with $|A\boldsymbol{\omega}| = \text{const}$: the Euler case $\mathbf{r} = 0$ where $f(\boldsymbol{\omega}) = 0$ reduces to the equation of the ellipsoid $T = h$; the case of steady rotations; finally, some particular cases of the Lagrange and Hess solutions, when the rigid body performs precessional motion around the vertical axis [Gorr & Iljukhin, 1974].

4. Topology of the Surfaces $\mathcal{P}^2_{h,l}$

Before we study the enveloping surfaces $\partial\mathcal{V}_{h,l} \subset \mathbb{R}^3(\boldsymbol{\omega})$, let us turn our attention to the somewhat simpler auxiliary two-dimensional surfaces

$$\begin{aligned} \mathcal{P}^2_{h,l} &= \{H = h,\, L = l,\, I = 1,\, F = 0\} \\ &\subset \mathcal{E}^3_{h,l} \subset \mathbb{R}^6(\boldsymbol{\omega}, \boldsymbol{\gamma}) , \end{aligned} \tag{28}$$

from which $\partial\mathcal{V}_{h,l}$ is obtained by the projection p. Because of the additional restriction $F = 0$, the surfaces $\mathcal{P}^2_{h,l}$ have a richer bifurcation scheme than $\mathcal{E}^3_{h,l}$. This section determines the classification of topologically distinct types of these surfaces, in their dependence on parameters and integral constants.

As usual, the critical points of the map $\mathcal{F}_1 = H \times L : M^4 \to \mathbb{R}^2(h, l)$, where M^4 is the surface $\{I = 1,\, F = 0\} \subset \mathbb{R}^6(\boldsymbol{\omega}, \boldsymbol{\gamma})$, are obtained from the condition $\mathrm{rank}(d\mathcal{F}_1) < 2$ or from the equivalent condition

$$\begin{aligned} \mu_1 \frac{\partial H}{\partial(\boldsymbol{\omega}, \boldsymbol{\gamma})} + \mu_2 \frac{\partial L}{\partial(\boldsymbol{\omega}, \boldsymbol{\gamma})} + \mu_3 \frac{\partial F}{\partial(\boldsymbol{\omega}, \boldsymbol{\gamma})} \\ + \mu_4 \frac{\partial I}{\partial(\boldsymbol{\omega}, \boldsymbol{\gamma})} = 0 , \end{aligned} \tag{29}$$

where μ_i are certain real coefficients. The derivatives by $\boldsymbol{\omega}$ and $\boldsymbol{\gamma}$ give, respectively, the two equations

$$\begin{aligned} \mu_1\boldsymbol{\omega} + \mu_2\boldsymbol{\gamma} + \mu_3\boldsymbol{\gamma}\times\mathbf{r} &= 0\,, \\ \mu_2 A\boldsymbol{\omega} - \mu_3 A\boldsymbol{\omega}\times\mathbf{r} + 2\mu_4\boldsymbol{\gamma} &= \mu_1\mathbf{r}\,. \end{aligned} \tag{30}$$

There exist three possible variants of solutions of (30):

(i) Let $\mu_4 \neq 0$. If the vectors $A\boldsymbol{\omega}$ and $\mathbf{r}$ are not collinear, then by comparing the second equation with $F = 0$, we find $\mu_3 = 0$. This means that the corresponding family of critical points is determined by the three integrals H, L, I only. Thus, the bifurcation set Σ of the momentum map $\mathcal{F} = H \times L$ is part of the bifurcation set of $\mathcal{F}_1$. The critical points of $\mathcal{F}$ always belong to a surface $\mathcal{P}^2_{h,l}$.

All other critical points and values of the map $\mathcal{F}_1$ are found with the assumption $A\boldsymbol{\omega} = \lambda\mathbf{r}$; the requirement that the linear Eqs. (30) be solvable for the μ_i leads to this condition.

(ii) Let $\mu_1 = \mu_2 = \mu_4 = 0$, $\mu_3 \neq 0$. From Eq. (29) we obtain $\partial F/\partial(\boldsymbol{\omega}, \boldsymbol{\gamma}) = 0$ or $A\boldsymbol{\omega}\times\mathbf{r} = \boldsymbol{\gamma}\times\mathbf{r} = 0$, i.e. the vectors $A\boldsymbol{\omega}$, $\mathbf{r}$, $\boldsymbol{\gamma}$ are collinear at a certain instant of time. Then the integrals L and I determine $\lambda = \pm l/|\mathbf{r}|$, $\boldsymbol{\gamma} = \pm\mathbf{r}/|\mathbf{r}|$, and with $H = h$ it follows that the critical values belong to the curves

$$h = \frac{l^2\langle A^{-1}\mathbf{r},\, \mathbf{r}\rangle}{2|\mathbf{r}|^2} \mp |\mathbf{r}|\,. \tag{31}$$

These curves contain the equilibrium points $(h, l) = (\mp|\mathbf{r}|, 0)$ where they are tangent to the curves (13). (In the special case $r_2 = r_3 = 0$ they are identical with the curves (17) of relative equilibria.)

(iii) Let $\mu_4 = 0$ and $\mu_1\mu_2\mu_3 \neq 0$. The corresponding family of critical points is determined by the three functions H, L, F and does not depend on the integral I. From the second equation of (30) it follows that the vectors $A\boldsymbol{\omega}$, $\mathbf{r}$ are collinear and that $\lambda = \mu_1/\mu_2$. Computing the scalar product of $\mathbf{r}$ and $\boldsymbol{\gamma}$ with the first equation of (30) leads to the two conditions

$$\begin{aligned} \lambda^2\langle A^{-1}\mathbf{r},\, \mathbf{r}\rangle + \langle\mathbf{r},\, \boldsymbol{\gamma}\rangle &= 0\,, \\ \lambda^2\langle A^{-1}\mathbf{r},\, \boldsymbol{\gamma}\rangle + 1 &= 0\,. \end{aligned} \tag{32}$$

Nonempty intersections of the planes (32) with the Poisson sphere allow us to obtain two critical points for every critical value. Combining (32) with the expressions (2) we find $l = -\lambda^3\langle A^{-1}\mathbf{r},\, \mathbf{r}\rangle$, $h = \frac{3}{2}\lambda^2\langle A^{-1}\mathbf{r},\, \mathbf{r}\rangle$, and the curve of critical values

$$8h^3 = 27l^2\langle A^{-1}\mathbf{r},\, \mathbf{r}\rangle$$

$$\text{with } h\text{-range} \qquad \frac{3\langle A^{-1}\mathbf{r},\, \mathbf{r}\rangle}{2|A^{-1}\mathbf{r}|} < h < \frac{3}{2}|\mathbf{r}|\,. \tag{33}$$

This piece of the bifurcation set of $\mathcal{P}^2_{h,l}$ disappears if all moments of inertia are equal or if two of the r_i vanish; then there exist critical points of cases (i) and (ii) only. Near the upper end $h = \frac{3}{2}|\mathbf{r}|$ of its range, the curve (33) connects to the curve (31), with $l^2 = |\mathbf{r}|^3/\langle A^{-1}\mathbf{r},\, \mathbf{r}\rangle$. Near the lower end it joins the piece $\sigma \in (A_1, \infty)$ of (13). An example is shown in the right part of Fig. 10 where curve (33) is the left boundary of the tiny black zone; it ends on the curve (31) at the upper white dot, and at the lower white dot it is tangent to the curve (14). The continuation of (33) down to $(h, l) = (0, 0)$ will be given an interpretation in Sec. 6, see Eq. (49).

All critical points on $\mathcal{P}^2_{h,l}$ of the map $\mathcal{F}_1 = H \times L : M^4 \to \mathbb{R}^2(h, l)$ have now been determined, and we have identified all corresponding critical values of the first integrals. The bifurcation set $\tilde{\Sigma}$ of the surfaces $\mathcal{P}^2_{h,l}$ consists not only of Σ, the set corresponding to relative equilibria, but in addition to the union of the curves (31) and (33).

Before we discuss the interpretation of these extra bifurcation lines, we establish an important connection between $\mathcal{P}^2_{h,l}$ and its projection $\tilde{\mathcal{U}}_{h,l}$ to the Poisson sphere which does not necessarily cover the entire energetically accessible region $\mathcal{U}_{h,l}$. Rather we have the following

Proposition 4.1. *The projection* $\pi : (\boldsymbol{\omega}, \boldsymbol{\gamma}) \mapsto \boldsymbol{\gamma}$ *maps the surface* $\mathcal{P}^2_{h,l}$ *into the domain* $\tilde{\mathcal{U}}_{h,l} \subset \mathcal{U}_{h,l}$ *on the Poisson sphere* $S^2(\boldsymbol{\gamma})$. *In local coordinates, this domain is defined by*

$$\tilde{\mathcal{U}}_{h,l} = \{\tilde{U}_l(\boldsymbol{\gamma}) \le h\} \subset S^2\,, \tag{34}$$

where

$$\tilde{U}_l(\boldsymbol{\gamma}) = \frac{l^2\langle A(\boldsymbol{\gamma}\times\mathbf{r}),\, \boldsymbol{\gamma}\times\mathbf{r}\rangle}{2\langle A\boldsymbol{\gamma}\times A(\boldsymbol{\gamma}\times\mathbf{r}),\, \boldsymbol{\gamma}\times(\boldsymbol{\gamma}\times\mathbf{r})\rangle} - \langle\mathbf{r},\, \boldsymbol{\gamma}\rangle\,. \tag{35}$$

The surface $\mathcal{P}^2_{h,l}$ *is a singular fiber bundle over* $\tilde{\mathcal{U}}_{h,l}$, *where the fiber over* $\boldsymbol{\gamma} \in \tilde{\mathcal{U}}_{h,l}$ *is*

(i) *a point* S^0 *if* $\boldsymbol{\gamma} \in \partial\tilde{\mathcal{U}}_{h,l}$
(ii) *a circle* S^1 *if* $\boldsymbol{\gamma} = \pm\mathbf{r}/|\mathbf{r}| =: \pm\hat{\mathbf{r}} \notin \partial\mathcal{U}_{h,l}$
(iii) *two points* $2S^0$ *otherwise.*

Proof. To find the relationship between the points of the surface $\mathcal{P}^2_{h,l}$ and the points of its image $\pi(\mathcal{P}^2_{h,l})$

on the Poisson sphere, fix the vector $\boldsymbol{\gamma}$ and consider first the case $\boldsymbol{\gamma} \times \mathbf{r} =: \mathbf{u} \neq 0$. Then the map $\pi|_{\mathcal{P}^2_{h,l}}$ on fibers is determined by the following formula:

$$A\boldsymbol{\omega} = \frac{\mathbf{u} \times (A\boldsymbol{\gamma} \times A\mathbf{u})l}{\langle A\boldsymbol{\gamma} \times A\mathbf{u},\, \boldsymbol{\gamma} \times \mathbf{u}\rangle} \pm \sqrt{2 \det A}(\boldsymbol{\gamma} \times \mathbf{u})\, \frac{\sqrt{2(h - \tilde{U}_l)(\boldsymbol{\gamma})}}{\sqrt{\langle A\boldsymbol{\gamma} \times A\mathbf{u},\, \boldsymbol{\gamma} \times \mathbf{u}\rangle}}\,, \tag{36}$$

where

$$\tilde{U}_l = \frac{l^2\langle A\mathbf{u},\, \mathbf{u}\rangle}{2\langle A\boldsymbol{\gamma} \times A\mathbf{u},\, \boldsymbol{\gamma} \times \mathbf{u}\rangle} - \langle \mathbf{r},\, \boldsymbol{\gamma}\rangle\,. \tag{37}$$

Equation (36) may be verified immediately by substitution in the expressions for H, L, F. Each point of the sphere at which the inequalities $\tilde{U}_l(\boldsymbol{\gamma}) < h$ and $\boldsymbol{\gamma} \times \mathbf{r} \neq 0$ are fulfilled, has exactly two pre-images on $\mathcal{P}^2_{h,l}$. Boundary points at which $\tilde{U}_l(\boldsymbol{\gamma}) = h$ have only one pre-image S^0 on $\mathcal{P}^2_{h,l}$.

In the alternative case $\boldsymbol{\gamma} = \pm\hat{\mathbf{r}}$, the fiber in $\mathcal{P}^2_{h,l}$ is a topological circle formed by the intersection of an ellipsoid with a plane (the integral levels $H = h$ and $L = l$). Finally, if $\boldsymbol{\gamma}$ belongs to the boundary of the domain of possible configurations $\partial\mathcal{U}_{h,l}$ then this circle collapses into a point. ■

The topological type of the surface $\mathcal{P}^2_{h,l}$ is uniquely determined by two factors: the structure of the domain $\tilde{\mathcal{U}}_{h,l} \subset S^2$ and the location of the *poles* $\boldsymbol{\gamma} = \pm\hat{\mathbf{r}}$ with respect to this domain. Let us call $\boldsymbol{\gamma} = \hat{\mathbf{r}}$ the "north pole", and $\boldsymbol{\gamma} = -\hat{\mathbf{r}}$ the "south pole" of the Poisson sphere. The north pole corresponds to the stable, the south pole to the unstable equilibrium position of the body. The topology of the boundary $\partial\tilde{\mathcal{U}}_{h,l}$ varies across the curves of Σ, together with the change of type of $\partial\mathcal{U}_{h,l}$, and — as will be discussed in connection with Fig. 12 — at the curve (33). The curves (31), on the other hand, indicate a change in the number of poles in the interior of $\tilde{\mathcal{U}}_{h,l}$. Thus Proposition 4.1 implies that the topological type of $\mathcal{P}^2_{h,l}$ changes at all values $(h,\, l) \in \tilde{\Sigma}$.

For illustration, Figs. 10–12 exhibit an example from the Grioli family [1947], i.e. $r_1\sqrt{A_3 - A_2} = r_2\sqrt{A_1 - A_3}$ with $r_1^2 + r_2^2 = 1$ and $r_3 = 0$. The left part of Fig. 10 shows the bifurcations sets Σ and $\tilde{\Sigma}$. The thick red, yellow and blue curves are given by (14), the thick green curve is from (16); these four curves are the set Σ. The two brown lines are the curves (31); the upper one just below the thick red line of stable relative equilibria, the lower one

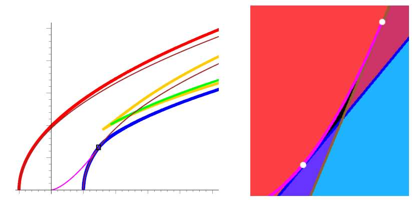

Fig. 10. (Left) Bifurcation diagram for $(A_1,\, A_2,\, A_3) = (2,\, 1,\, 1.1)$ and $(r_1,\, r_2,\, r_3) = (0.94868,\, 0.31623,\, 0)$. The curves are identified in the text. (Right) Schematic representation of the right part of Fig. 11.

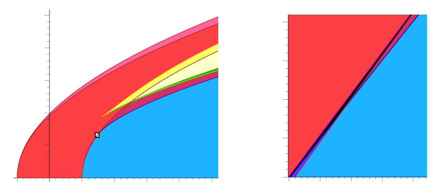

Fig. 11. (Left) Color code for the regions of different topological type of $\mathcal{P}^2_{h,l}$, with the same parameters as in Fig. 10. (Right) Blow-up of the tiny rectangle near $h = 1.5$.

almost indistinguishably below the blue line — up to values of $(h,\, l)$ near $(1.5,\, 1.348)$ where it crosses over to the neighborhood of the yellow line. The details of this crossing over are shown in the blow-ups (at right) of the tiny rectangles in Figs. 10 and 11. The scenario involves the curve (33) which is the arc connecting the two white dots, to the left of the black zone. The continuation of curve (33) down to the point $(h,\, l) = (0,\, 0)$ is shown in magenta color for reasons discussed in Sec. 6.

In the left part of Fig. 11 we use a color code to identify the topologies of $\mathcal{E}^3_{h,l}$ and $\mathcal{P}^2_{h,l}$ in the regular zones defined by $\tilde{\Sigma}$. The energy surface is S^3 in four regions with different types of $\mathcal{P}^2_{h,l}$. Using the notation M^2_i for an oriented two-manifold with genus i, we have $\mathcal{P}^2_{h,l}$ of types $S^2 = M^2_0$ (pale red, between the thick red and the upper brown line), $T^2 = M^2_1$ (bright red), M^2_2 (magenta, to the right of the lower brown line, between the blue and yellow lines of relative equilibria), and M^2_3 (black, only visible in the schematic drawing in the right part of Fig. 10).

The yellow and green lines enclose two zones of different energy surfaces. In the upper part $\mathcal{E}^3_{h,l}$ consists of two disjoint S^3; in one of them $\mathcal{P}^2_{h,l}$ is always T^2, in the other it changes from S^2 in the darker yellow region (between the upper yellow and the brown line) to T^2 in the pale yellow region. In the thin lower part between the yellow and green

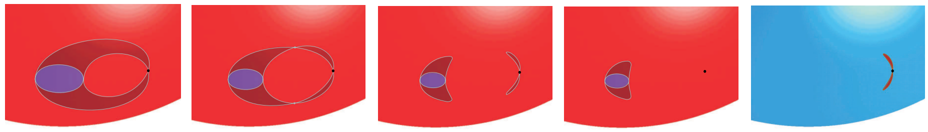

Fig. 12. The neighborhood of the south pole $\boldsymbol{\gamma} = -\hat{\mathbf{r}}$ (black dot) on the Poisson sphere, for five pairs of $(h,\, l)$ taken from the right part of Fig. 11. The deep blue ellipse is not covered by $\mathcal{U}_{h,l}$, brown is the part of $\mathcal{U}_{h,l}$ which does not belong to $\tilde{\mathcal{U}}_{h,l}$. From left to right: $(h,\, l) = (1.473,\, 1.313)$, $(1.47357,\, 1.312922)$, $(1.472,\, 1.3105)$, $(1.4772,\, 1.317)$, $(1.4652,\, 1.301)$.

lines, $\mathcal{E}^3_{h,l}$ is $S^1 \times S^2$; the surface $\mathcal{P}^2_{h,l}$ is M^2_2 to left of line (31) and M^2_3 to its right. Finally, below the blue line, the energy surface is $\mathbb{R}P^3$, with $\mathcal{P}^2_{h,l}$ of type T^2 in the sky blue region (the main part of the blue zone), and M^2_2 in the dark azure (visible only in the right part of Fig. 10).

How do we obtain these assertions? Let us first ignore the complications introduced by curve (33). Then for each connected piece of $\tilde{\mathcal{U}}_{h,l} \subset \mathcal{U}_{h,l}$ we must consider the location of the poles $\boldsymbol{\gamma} = \pm\hat{\mathbf{r}}$. If they are both outside of $\mathcal{U}_{h,l}$, then $\tilde{\mathcal{U}}_{h,l}$ is homeomorphic to $\mathcal{U}_{h,l}$, and if the latter is a disk with zero, one or two holes, then Proposition 4.1 tells us that the surface $\mathcal{P}^2_{h,l}$ is, respectively, S^2, T^2 or M^2_2. Now, in a small strip below the thick red bifurcation line, the north pole lies outside $\mathcal{U}_{h,l}$; the axis of rotation in the stable relative equilibrium is *not* in the direction of $\hat{\mathbf{r}}$. The north pole enters $\mathcal{U}_{h,l}$ when $U_l(\hat{\mathbf{r}}) = h$ which happens along the parabola

$$h = \frac{l^2}{2\langle A\hat{\mathbf{r}},\, \hat{\mathbf{r}}\rangle} - |\mathbf{r}|\,. \tag{38}$$

But this lies *above* the upper brown curve (31) because

$$\langle A\hat{\mathbf{r}},\, \hat{\mathbf{r}}\rangle\langle A^{-1}\hat{\mathbf{r}},\, \hat{\mathbf{r}}\rangle \geq 1\,. \tag{39}$$

On the other hand, when $\boldsymbol{\gamma} = \pm\hat{\mathbf{r}}$ we have $F = 0$, hence poles inside $\mathcal{U}_{h,l}$ belong to $\tilde{\mathcal{U}}_{h,l}$ as well: As long as we stay above curve (31), $\boldsymbol{\gamma} = \hat{\mathbf{r}}$ remains a point of the boundary $\partial\tilde{\mathcal{U}}_{h,l}$. In fact, the boundary has a self-intersection at that point, a singularity of the projection $\partial\tilde{\mathcal{U}}_{h,l}$, not of $\mathcal{P}^2_{h,l}$.

A topological change of $\mathcal{P}^2_{h,l}$ occurs when the map $\mathcal{F}_1$ has a critical point. This happens at the upper curve (31) where the north pole enters the interior of $\tilde{\mathcal{U}}_{h,l}$. From then on, $\mathcal{P}^2_{h,l}$ has an additional handle because two inner points are replaced by a connecting circle S^1. The surface is oriented because it divides its component of $\mathcal{E}^3_{h,l}$ into two disjoint pieces, corresponding to the two signs of (27). Therefore, S^2 turns into T^2.

In other examples, the topology of $\tilde{\mathcal{U}}_{h,l}$ may be that of an annulus, or a disk with a hole. As long as no pole is in its interior, $\mathcal{P}^2_{h,l}$ is a torus T^2, but when $\hat{\mathbf{r}}$ (or $-\hat{\mathbf{r}}$) enters, it is a manifold M^2_2 of genus 2. Similarly, if $\tilde{\mathcal{U}}_{h,l}$ were a disk with two holes and no pole inside, $\mathcal{P}^2_{h,l}$ would be a manifold M^2_2 (we have no example for that and believe it does not exist). However, with one interior pole, it would be a manifold M^2_3 (and there are examples of that, e.g. in the Kovalevskaya case).

The interpretation of the lower brown curve (31) is that when it is crossed from left to right, the south pole $\boldsymbol{\gamma} = \hat{\mathbf{r}}$ enters the interior of $\tilde{\mathcal{U}}_{h,l}$. This adds another handle to $\mathcal{P}^2_{h,l}$, see Table 1 for a summary. Its first three rows describe the possible cases without the complications added by the existence of a curve (33). (The question mark at the upper right entry refers to our conjecture that this case does not exist.) The first column refers to $\tilde{\mathcal{U}}_{h,l}$ being the entire Poisson sphere; it must then contain both poles. Without them, $\mathcal{P}^2_{h,l}$ would consist of two separate spheres S^2, but the S^1 pre-images of the two poles connect these spheres by two handles and thereby generate a torus T^2.

The last row in Table 1 adds what happens when the curve (33) enters the game. Together with other bifurcation lines it forms a zone where the genus of $\mathcal{P}^2_{h,l}$ is further increased. We believe that the highest possible genus that can be obtained this way is 5. As an example, we give the set of parameters $(A_1,\, A_2,\, A_3) = (4,\, 2.99,\, 1.02)$, $\mathbf{r} = (\sqrt{0.5},\, \sqrt{0.5},\, 0)$, $(h,\, l) = (1.49229,\, 1.83563)$. In the case of Figs. 10 and 11 the extra zone introduced by the curve (33) is the black triangle that it forms with the curves (31) and (14). It lies inside the region where the energy surface is a three-sphere S^3. Hence, $\mathcal{P}^2_{h,l}$ is a manifold M^2_3 of genus 3.

The mechanism associated with the curve (33) is illustrated in Fig. 12 for the example in Figs. 10 and 11 where it occurs at the transition of $\mathcal{E}^3_{h,l}$ from S^3 to $\mathbb{R}P^3$. The five pictures show the neighborhood

Table 1. Possible types of the topology of $\mathcal{P}^2_{h,l}$, depending on topology of the energy surface $\mathcal{E}^3_{h,l}$ (four columns) and the nature of its projection $\tilde{\mathcal{U}}_{h,l}$ to the Poisson sphere in relation to the poles $\pm\hat{\mathbf{r}}$ (four rows).

	Topology of $\mathcal{E}^3_{h,l}$			
	$\mathbb{R}P^3$	S^3	$S^1 \times S^2$	$(S^1 \times S^2)\#(S^1 \times S^2)$
	Nature of $\mathcal{U}_{h,l}$			
Nature of $\tilde{\mathcal{U}}_{h,l}$ ↓	S^2	D^2	$S^2\backslash 2D^2$	$S^2\backslash 3D^2$
no pole inside	–	S^2	T^2	M^2_2 ?
$\hat{\mathbf{r}}$ inside	–	T^2	M^2_2	M^2_3
$\hat{\mathbf{r}}$ and $-\hat{\mathbf{r}}$ inside	T^2	M^2_2	M^2_3	M^2_4
two separate holes at $-\hat{\mathbf{r}}$	M^2_2	M^2_3	M^2_4	M^2_5

of the south pole $\boldsymbol{\gamma} = -\hat{\mathbf{r}}$ of the Poisson sphere, for five different values $(h,\, l)$. The four images on left are cases where $\mathcal{E}^3_{h,l}$ is S^3, the image on right is a case where $\mathcal{E}^3_{h,l}$ is $\mathbb{R}P^3$. The bright red color shows $\tilde{\mathcal{U}}_{h,l}$, brown is the difference $\mathcal{U}_{h,l}\backslash\tilde{\mathcal{U}}_{h,l}$; the dark blue ellipse is an inaccessible part of the Poisson sphere. The south pole is shown as a black dot. It is a boundary point of $\tilde{\mathcal{U}}_{h,l}$ in the three images on left which are all for $(h,\, l)$ to the left of line (31). The leftmost picture corresponds to $(h,\, l)$ from the red region in Fig. 11; $\mathcal{P}^2_{h,l}$ is of type T^2 as the north pole lies inside $\tilde{\mathcal{U}}_{h,l}$ and the south pole is a boundary point. The second image from left is for $(h,\, l)$ on line (33); we see how the brown region is pinched at two points. Next, in the third image, where $(h,\, l)$ is from the tiny black region in Fig. 11, the south pole is still a boundary point of $\tilde{\mathcal{U}}_{h,l}$, but now it separates the two interior pieces of $\mathcal{U}_{h,l}\backslash\tilde{\mathcal{U}}_{h,l}$ forming a figure eight. Hence $\mathcal{P}^2_{h,l}$ has two additional handles and is of type M^2_3. The last red image is for $(h,\, l)$ from the magenta region in Fig. 11; here figure eight has disappeared (two handles less), but the south pole has entered the interior of $\tilde{\mathcal{U}}_{h,l}$ (one handle more), so the topology is of type M^2_2.

The blue image on right is for the dark azure region in Fig. 11 where the energy surface is $\mathbb{R}P^3$. The set $\tilde{\mathcal{U}}_{h,l}$ has two holes on the Poisson sphere, separated by the boundary point $-\hat{\mathbf{r}}$, so the topology of $\mathcal{P}^2_{h,l}$ is again M^2_2. Crossing the line (31) into the sky blue region of Fig. 11, the holes disappear, but the south pole becomes an inner point, so the topology becomes that of T^2.

So what happens along the curve (33)? A single hole of $\tilde{\mathcal{U}}_{h,l}$ (left image in Fig. 12) is splashed into three (middle image), increasing the genus of $\mathcal{P}^2_{h,l}$ by two. The south pole $\boldsymbol{\gamma} = -\hat{\mathbf{r}}$ is an essential part of this scenario, hence it appears that the transition can only take place from the second to the fourth row of Table 1.

A comprehensive survey on such bifurcation schemes of surfaces $\mathcal{P}^2_{h,l}$ — for all possible values of parameters A_i and r_i — has not been worked out yet, but it is unlikely that types other than those discussed in this paper will be found. Curves (31) and (33) have the same structure for all values of the parameters, and the singular points of $\mathcal{P}^2_{h,l}$ have been determined here in full generality. Hence it is hard if not impossible to conceive of a situation where $\mathcal{P}^2_{h,l}$ would be of type M^2_6.

The following section reviews Katok's analysis [1972] of the special cases $r_2 = r_3 = 0$ and relates it to the properties of the surfaces $\mathcal{P}^2_{h,l}$.

5. The Katok Cases $r_2 = r_3 = 0$

Katok [1972] gave a complete list of bifurcation diagrams for the special cases $r_2 = r_3 = 0$. Without loss of generality we may take $r_1 = 1$ and scale the moments of inertia with A_1 so that $(\alpha,\, \beta) := (A_2/A_1,\, A_3/A_1)$ are the two relevant parameters of the system. The physical restrictions $A_i + A_j \geq A_k$ determine the boundaries of the diagram in Fig. 13: the line $\alpha + \beta = 1$ corresponds to planar mass distribution in the body-fixed (2, 3)-plane; the lines $\beta = \pm 1 + \alpha$ represent planar mass distribution in the (1, 2)- and (1, 3)-planes, respectively. Bodies symmetric with respect to the 1, 2 and 3 axes are, respectively, located on the lines $\alpha = \beta$, $\alpha = 1$, and $\beta = 1$. No immediate physical interpretation can

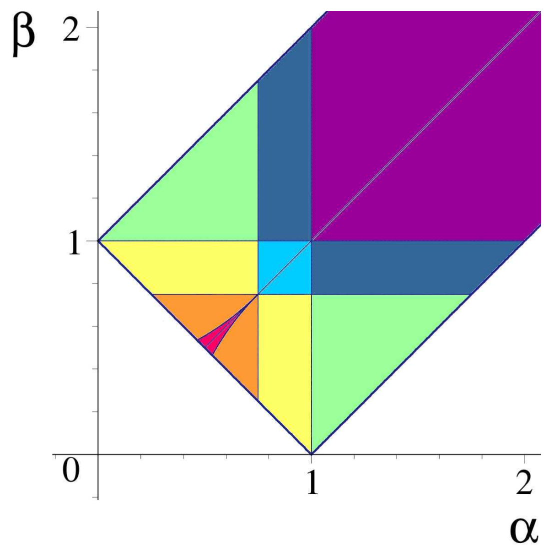

Fig. 13. Katok's partition of the (α, β)-plane into seven color coded regions, corresponding to different types of bifurcation diagrams. For later reference, the regions are called K1-red, K2-orange, K3-yellow, K4-green, K5-light blue, K6-blue, K7-violet.

be given to the further subdivision induced by the lines $\alpha = 3/4$, $\beta = 3/4$, as well as

$$\alpha = \frac{9 - 8\beta}{(5 - 4\beta)^2}, \quad \beta \in \left(\beta_0, \frac{3}{4}\right),$$

$$\text{and} \qquad \beta = \frac{9 - 8\alpha}{(5 - 4\alpha)^2}, \quad \alpha \in \left(\alpha_0, \frac{3}{4}\right), \tag{40}$$

where $\alpha_0 = \beta_0 \approx 0.4647$. (The last line is not mentioned in [Katok, 1972]; it is obtained from the conditions that both curves (18), with $i = 2$ and $i = 3$, have cusps, and that the starting point of the curve with $i = 3$, i.e. $\mu^2 = \alpha_3/r_1$, coincides with the intersection of the curve (18), $i = 2$, and (17).) Altogether there are seven regions in parameter space with bifurcation diagrams of different type. We shall denote them as K1,…,K7, see the caption of Fig. 13.

The seven types of bifurcation diagrams are shown in Figs. 14 and 15. In each diagram the lines of relative equilibria (17) and (18) delimit regions with different topology of $\mathcal{E}^3_{h,l}$ and $\mathcal{P}^2_{h,l}$. The lines (31) are identical with (17), and line (33) disappears. (But notice we have included line (49), to be explained in the following section; it marks the distinction between $\nu(\partial\mathcal{V}_{h,l}) = 1$ or 3 in the first entry of the last column.) Hence the sets $\tilde{\mathcal{U}}_{h,l}$ are homeomorphic to $\mathcal{U}_{h,l}$ in all cases, and for each type of energy surface $\mathcal{E}^3_{h,l}$ there is only one type of $\mathcal{P}^2_{h,l}$. Katok numbered them from I to VII; we use a color code to exhibit this classification. Table 2 summarizes the results. The fourth column gives the topological type of $\mathcal{P}^2_{h,l}$ which implies a further refinement of Katok's types II and III.

Notice that K1 is the only parameter region where all seven types occur. We take the example $(1.7, 0.9, 0.86) \in$ K1 (first image in Fig. 15) to illustrate the effective potential $U_l(\boldsymbol{\gamma})$ on the Poisson sphere, for different values of the angular momentum l. There are eight different cases, as shown in Fig. 16. The north pole $\hat{\mathbf{r}}$ marks the minimum of the effective potential; its direction is indicated by the dot on the left backside of each sphere. The south pole $-\hat{\mathbf{r}}$ is at the right front. All images possess symmetry with respect to reflection of the 2 and 3 axes. The colors code for the topological types I–VII of the energy surfaces $\mathcal{E}^3_{h,l}$: when $h = U_l(\boldsymbol{\gamma})$ with $\boldsymbol{\gamma}$ from a region with a certain color, then we may use Table 2 to read off the type of $\mathcal{E}^3_{h,l}$ and the corresponding $\mathcal{P}^2_{h,l}$. (The type IV is not represented in these images because h is then larger than the maximum of the effective potential).

It is instructive to relate the topology of $\mathcal{E}^3_{h,l}$ and $\mathcal{P}^2_{h,l}$ to the foliation of the Poisson sphere by level lines of $U_l(\boldsymbol{\gamma})$, using the technique of Reeb graphs [Bolsinov & Fomenko, 1999] for Morse functions on the sphere. The level lines may be interpreted as orbits of a Hamiltonian system with phase space $S^2(\boldsymbol{\gamma})$. Representing each level line as a point on a graph where h is the vertical coordinate, we obtain the diagrams of Fig. 17. The black graphs show how the level lines are connected. Each branch represents a continuous family of level lines. Lower end points correspond to local energy minima, upper end points to local maxima. The north pole is marked with a white, the south pole with a black dot. Branch points correspond to saddles and separatrices in the system of equipotential lines. (The saddles come in pairs, either on the (1, 2)- or the (1, 3)-meridians of the Poisson sphere.) Using these Reeb graphs it is possible to construct the corresponding Fomenko molecules, see [Bolsinov & Fomenko, 1999].

6. Structure and Bifurcations of the Enveloping Surfaces in $\boldsymbol{\omega}$-Space

In the preceding section we determined the structure of the surfaces $\mathcal{P}^2_{h,l}$ in $\mathbb{R}^6(\boldsymbol{\omega}, \boldsymbol{\gamma})$. Their projections to the space of angular velocities are the

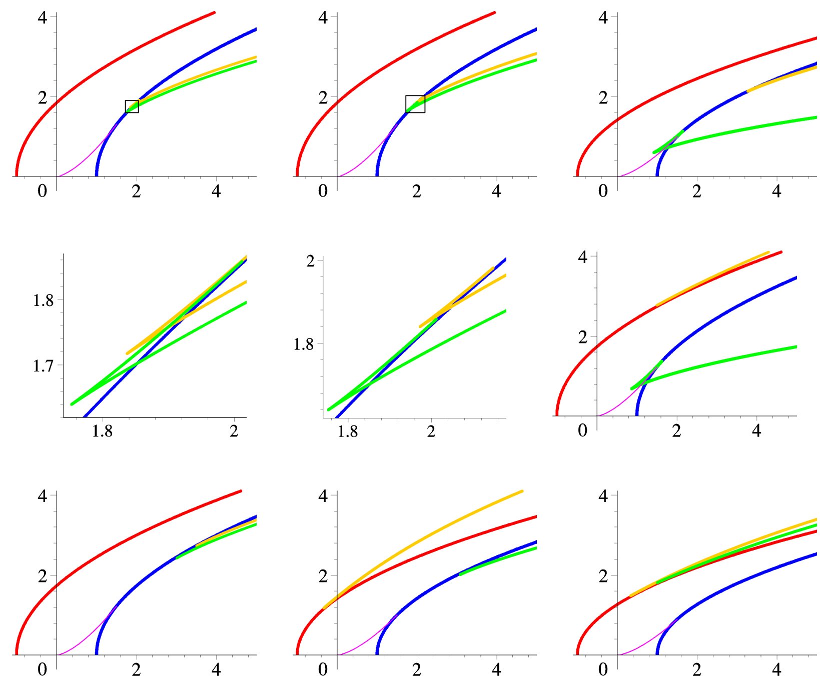

Fig. 14. The seven types of bifurcation diagrams for $\hat{\mathbf{r}} = (1, 0, 0)$. The moments of inertia (A_1, A_2, A_3) are the following. Upper row: $(1.7, 0.9, 0.86) \in$ K1, $(1.7, 0.96, 0.86) \in$ K2, $(1.0, 0.78, 0.2201) \in$ K3; middle row: the first two images are blow-ups of the diagrams above, then $(1.5, 1.8, 0.301) \in$ K4; bottom row: $(1.5, 1.2, 1.126) \in$ K5, $(1.0, 1.75, 0.76) \in$ K6, $(0.8, 1.1, 1.0) \in$ K7.

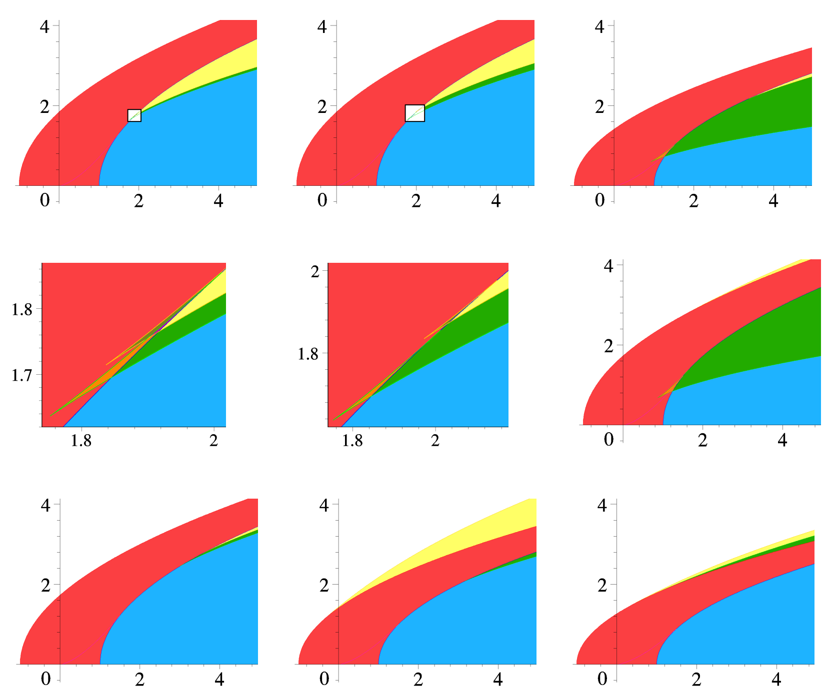

Fig. 15. The bifurcation diagrams for the same parameters as in Fig. 14, with color code of Table 2 for the seven different types of energy surfaces $\mathcal{E}^3_{h,l}$.

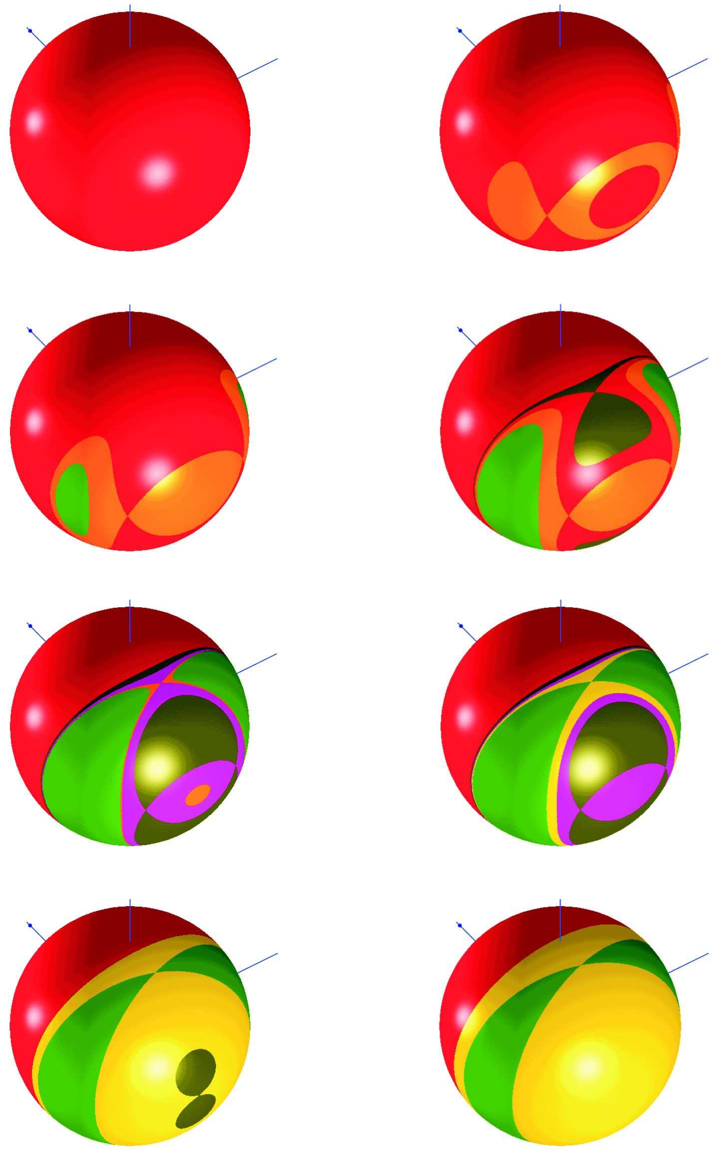

Fig. 16. The eight different types of effective potentials for $(r_1, r_2, r_3) = (1, 0, 0)$ and $(A_1, A_2, A_3) = (1.7, 0.9, 0.86) \in$ K1. The values of the angular momentum l are, from upper left to lower right, $l = 0$, $l = 1.68$, $l = 1.71$, $l = 1.74$, $l = 1.763$, $l = 1.773$, $l = 1.86$, $l = 2.0$. The colors correspond to those in Fig. 15.

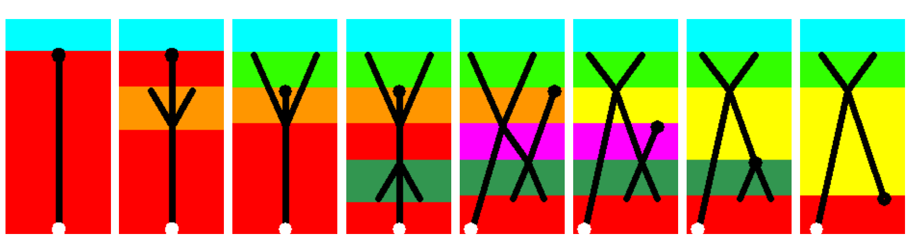

Fig. 17. Reeb graph representation of the eight types of energy surfaces for $\mathbf{r} = (1, 0, 0)$ and $(A_1, A_2, A_3) = (1.7, 0.9, 0.86) \in$ K1. Each point of the graph corresponds to an equipotential line $U_l(\boldsymbol{\gamma}) = h$; the energy h increases along the vertical. The bifurcation scheme of these graphs determines the topological type of $\mathcal{E}^3_{h,l}$ and $\mathcal{P}^2_{h,l}$, as indicated by the colors. The values of l are the same as in Fig. 16.

Table 2. The seven types of energy surfaces $\mathcal{E}^3_{h,l}$ in the Katok family of rigid bodies, and the corresponding Poincaré surfaces of section $\mathcal{P}^2_{h,l}$. The last column gives the number of singularities of the projections $\partial\mathcal{V}_{h,l}$ on the line where $\boldsymbol{\gamma}$ is collinear with $\mathbf{l} = A\boldsymbol{\omega}$, see Sec. 6.

	Color	$\mathcal{E}^3_{h,l}$	$\mathcal{P}^2_{h,l}$	$\nu(\partial\mathcal{V}_{h,l})$
I		S^3	T^2	1 or 3
II		$S^3 \cup S^3$	$T^2 \cup T^2$ if $A_2 < A_1$ and $A_3 < A_1$	1 and 1
			$S^2 \cup S^2$ if $A_2 > A_1$ or $A_3 > A_1$	0 and 0
III		$S^1 \times S^2$	M^2_3 if $A_2 < A_1$ or $A_3 < A_1$	2
			T^2 if $A_2 > A_1$ and $A_3 > A_1$	0
IV		$\mathbb{R}P^3$	T^2	2
V		$(S^1 \times S^2)\#(S^1 \times S^2)$	M^2_3	1
VI		$S^3 \cup S^3 \cup S^3$	$S^2 \cup S^2 \cup T^2$	0, 0 and 1
VII		$S^3 \cup (S^1 \times S^2)$	$T^2 \cup T^2$	1 and 0

enveloping surface in which we are interested, $\partial\mathcal{V}_{h,l} = p(\mathcal{P}^2_{h,l}) \subset \mathbb{R}^3(\boldsymbol{\omega})$. As mentioned in (26), the envelopes are characterized by $f(\boldsymbol{\omega}) = 0$, hence their singular points are given by the two conditions

$$f(\boldsymbol{\omega}) = 0 \quad \text{and} \quad \frac{\partial f(\boldsymbol{\omega})}{\partial \boldsymbol{\omega}} = 0\,. \tag{41}$$

Using Eq. (22), we may write the latter condition as

$$\eta_1 A\boldsymbol{\omega} + \eta_2 \mathbf{r} + \eta_3 \boldsymbol{\omega} = 0, \tag{42}$$

where

$$\begin{aligned} \eta_1 &= |\mathbf{r}|^2 - (T-h)^2\,, \\ \eta_2 &= (T-h)l - \langle A\boldsymbol{\omega},\, \mathbf{r}\rangle\,, \\ \eta_3 &= \langle A\boldsymbol{\omega},\, \mathbf{r}\rangle l - (T-h)|A\boldsymbol{\omega}|^2\,. \end{aligned} \tag{43}$$

Equation (42) may be read as a set of linear equations for the η_i; the matrix of coefficients has determinant $\langle A\boldsymbol{\omega} \times \mathbf{r},\, \boldsymbol{\omega}\rangle$. If this determinant is nonzero, then $\eta_1 = \eta_2 = \eta_3 = 0$ is the only solution, and with (43) we find $|A\boldsymbol{\omega}|^2 = l^2$, $\langle A\boldsymbol{\omega},\, \mathbf{r}\rangle = \pm|\mathbf{r}|l$. It follows that the vector of the angular momentum is collinear with $\mathbf{r}$, $A\boldsymbol{\omega} = \lambda\mathbf{r}$, since $|A\boldsymbol{\omega} \times \mathbf{r}|^2 = |A\boldsymbol{\omega}|^2|\mathbf{r}|^2 - \langle A\boldsymbol{\omega},\, \mathbf{r}\rangle^2 = 0$. Notice that $|A\boldsymbol{\omega}| = l$ means $\mathbf{l}^2 := |A\boldsymbol{\omega}|^2$ assumes its smallest possible value.

On the other hand, for nontrivial solutions η_i of (42) to exist, the determinant must vanish, $\langle A\boldsymbol{\omega} \times \mathbf{r},\, \boldsymbol{\omega}\rangle = 0$. Now there are two possibilities. First, let $\eta_3 = 0$. Then, with the help of (42), we obtain again $A\boldsymbol{\omega} = \lambda\mathbf{r}$. The second possible situation, $A\boldsymbol{\omega} \times \mathbf{r} \neq 0$ and $\eta_3 \neq 0$, will be considered below.

Consider the first possibility, where $A\boldsymbol{\omega}$ and $\mathbf{r}$ are collinear, i.e. $\boldsymbol{\omega}$ lies on the axis with unit vector $\mathbf{e} := A^{-1}\mathbf{r}/|A^{-1}\mathbf{r}|$. Inserting $A\boldsymbol{\omega} = \lambda\mathbf{r}$ into the first integrals (2), we find that the coefficient λ must be a real solution of the cubic equation

$$\frac{1}{2}\,\langle A^{-1}\mathbf{r},\, \mathbf{r}\rangle\lambda^3 - h\lambda - l = 0\,, \tag{44}$$

while $\boldsymbol{\gamma}$ satisfies the equations

$$\lambda\langle\mathbf{r},\, \boldsymbol{\gamma}\rangle = l \quad \text{and} \quad |\boldsymbol{\gamma}| = 1\,, \tag{45}$$

i.e. it lies on the intersection of the Poisson sphere with a plane normal to $\mathbf{r}$. Depending on the number and values of the real solutions of (44), the closed domain $\mathcal{V}_{h,l} \subset \mathbb{R}^3(\boldsymbol{\omega})$ may have 0, 1, 2, or 3, but no more than three distinct points on the $\mathbf{e}$ axis. These points of intersection are singular points of the real surface $\partial\mathcal{V}_{h,l}$. In the generic case, the tangents to this surface at such a singular point form a cone since the matrix of the second partial derivatives of $f(\boldsymbol{\omega})$ is nondegenerate.

The alternative possibility for a point of $\partial\mathcal{V}_{h,l}$ to be singular is that $A\boldsymbol{\omega} \times \mathbf{r} \neq 0$ and $\eta_3 \neq 0$. Then the decompositions $\boldsymbol{\gamma} = \zeta_1 A\boldsymbol{\omega} + \zeta_2\mathbf{r}$ and $\eta_3\boldsymbol{\omega} = -\eta_1 A\boldsymbol{\omega} - \eta_2\mathbf{r}$ together with the simple identities

$$(T-h)f = (\eta_1\zeta_2 - \eta_2\zeta_1)|A\boldsymbol{\omega}\times\mathbf{r}|^2\,,$$
$$\langle A\boldsymbol{\omega},\,\mathbf{r}\rangle f = -(\eta_2+\eta_3\zeta_1)|A\boldsymbol{\omega}\times\mathbf{r}|^2\,, \tag{46}$$

lead to the following expressions:

$$\boldsymbol{\omega}\times\boldsymbol{\gamma} = \frac{(h-T)f}{\eta_3|A\boldsymbol{\omega}\times\mathbf{r}|^2}\,(A\boldsymbol{\omega}\times\mathbf{r}) = 0\,,$$

$$A\boldsymbol{\omega}\times\boldsymbol{\omega} + \mathbf{r}\times\boldsymbol{\gamma} = \frac{\langle A\boldsymbol{\omega},\,\mathbf{r}\rangle f}{\eta_3|A\boldsymbol{\omega}\times\mathbf{r}|^2}\,(A\boldsymbol{\omega}\times\mathbf{r}) = 0\,. \tag{47}$$

Hence, in this case the singular points of $\partial\mathcal{V}_{h,l}$ turn out to be the relative equilibria of the system (1). The change in topological type of $\mathcal{E}^3_{h,l}$ upon passage through the bifurcation set $\Sigma\subset\mathbb{R}^2(h,\,l)$ discussed in Sec. 2, leads to a topological change of $\mathcal{V}_{h,l}$ as well. The steady rotations of the body around the vertical axis correspond to singularities of the enveloping surface $\partial\mathcal{V}_{h,l}$.

Disregarding these critical cases, we have the following

Proposition 6.1. *Let $\mathcal{P}^2_{h,l}$ be a regular surface of the level sets (28) and $\partial\mathcal{V}_{h,l} = p(\mathcal{P}^2_{h,l})\subset\mathbb{R}^3(\boldsymbol{\omega})$ its projection to the space of angular velocities. Then a fiber in $\mathcal{P}^2_{h,l}\subset\mathcal{E}^3_{h,l}$ over $\boldsymbol{\omega}\in\partial\mathcal{V}_{h,l}$ is either a circle S^1 (if $\boldsymbol{\omega}$ lies on the $\mathbf{e}$ axis) or a point S^0 (otherwise).*

Proof. If the vectors $A\boldsymbol{\omega}$, $\mathbf{r}$ are not collinear then, following (19), the vector $\boldsymbol{\gamma}$ is uniquely determined by the formula $\boldsymbol{\gamma} = \zeta_1 A\boldsymbol{\omega} + \zeta_2\mathbf{r}$. If, however, the point $\boldsymbol{\omega}\in\partial\mathcal{V}_{h,l}$ lies on the $\mathbf{e}$ axis, then $\boldsymbol{\gamma}$ fulfills (45), where the constant coefficient λ is a real solution of Eq. (44). A nonempty intersection of the unit sphere with the plane forms a circle $S^1\subset\mathbb{R}^3(\boldsymbol{\gamma})$. To prove that all points of this circle belong to the domain $\tilde{\mathcal{U}}_{h,l}\subset\mathcal{U}_{h,l}$, we use $\lambda\langle\mathbf{r},\,\boldsymbol{\gamma}\rangle = l$ and (44) to transform (37) into the expression

$$h - \tilde{U}_l(\boldsymbol{\gamma})|_{S^1} = \frac{\lambda^2\langle\boldsymbol{\gamma}\times A^{-1}\mathbf{r},\,\mathbf{u}\rangle^2}{2\langle A\boldsymbol{\gamma}\times A\mathbf{u},\,\boldsymbol{\gamma}\times\mathbf{u}\rangle}\,. \tag{48}$$

Non-negativity of the right-hand side means that the circle does not intersect $\partial\tilde{\mathcal{U}}_{h,l}$ but may touch it. Thus, the fiber over the given point $\boldsymbol{\omega}\in\partial\mathcal{V}_{h,l}$ is S^1. ■

Let us wrap up what we can say about the topology of the enveloping surfaces $\partial\mathcal{V}_{h,l}$. Of course it depends on the values (h,l) and the parameters of the rigid body. There exist regular surfaces $\partial\mathcal{V}_{h,l}$ which have no singular points — homeomorphic, for example, to the sphere S^2 or the torus T^2, see Fig. 21. Then, every connected component of $\mathcal{V}_{h,l}$ is a compact manifold with boundary. Singular surfaces $\partial\mathcal{V}_{h,l}$ occur at bifurcations of the energy surface, but not only there. There exist zones where for every pair of values (h,l) the enveloping surface has singular points on the $\mathbf{e}$-axis. The corresponding connected components of $\mathcal{V}_{h,l}$ are then "almost" manifolds with boundary, i.e. they are compact manifolds with boundary, but the boundary $\partial\mathcal{V}_{h,l}$ has 1, 2 or 3 singularities on the line $A\boldsymbol{\omega} = \lambda\mathbf{r}$. All examples of Figs. 18 through 20 possess components of this kind. We denote the number of these singular points by $\nu(\partial\mathcal{V}_{h,l})$. It can change in two ways. First, the number of real roots of Eq. (44) may change. This happens along the line where the discriminant of that equation vanishes:

$$8h^3 - 27l^2\langle A^{-1}\mathbf{r},\,\mathbf{r}\rangle = 0$$

in the h-range $\qquad 0\le h\le \frac{3}{2}\,|\mathbf{r}|\,. \qquad (49)$

This agrees with line (33) except for the larger h-range. The second way for the number of singular points to change is that real solutions λ of (44) may or may not be compatible with the inequalities $-|\mathbf{r}|\le\langle\mathbf{r},\,\boldsymbol{\gamma}\rangle\le|\mathbf{r}|$ which hold on the Poisson sphere. The changes happen at the two lines

$$\frac{1}{2}\,\langle A^{-1}\mathbf{r},\,\mathbf{r}\rangle\lambda^2 - h = \pm|\mathbf{r}|\,. \tag{50}$$

Using (44) it is straightforward to see that these are the lines (31).

The bifurcation diagram of the enveloping surfaces $\partial\mathcal{V}_{h,l}$ is therefore the union of $\tilde{\Sigma}$ and the line (49). The topological type of $\partial\mathcal{V}_{h,l}$ is that of $\mathcal{P}^2_{h,l}$ except for the singularities where circles on $\mathcal{P}^2_{h,l}$ have collapsed to points. The numbers $\nu(\partial\mathcal{V}_{h,l})$ are given in the last column of Table 2.

We formulate the main result as a theorem:

Theorem 6.2. *For fixed constants $(h,\,l)$ all trajectories which correspond to the solutions $\boldsymbol{\omega} = \boldsymbol{\omega}(t)$ of the vector Eq. (23) belong to the three-dimensional domain $\mathcal{V}_{h,l} = p(\mathcal{E}^3_{h,l})$. This domain has the following properties*:

(a) *an arbitrary point of $\mathcal{V}_{h,l}\backslash\partial\mathcal{V}_{h,l}$ has exactly two pre-images on the manifold $\mathcal{E}^3_{h,l}$*;
(b) *all singular points of the enveloping surfaces $\partial\mathcal{V}_{h,l}$ either correspond to relative equilibria or belong to the axis with unit vector* $\mathbf{e}$;

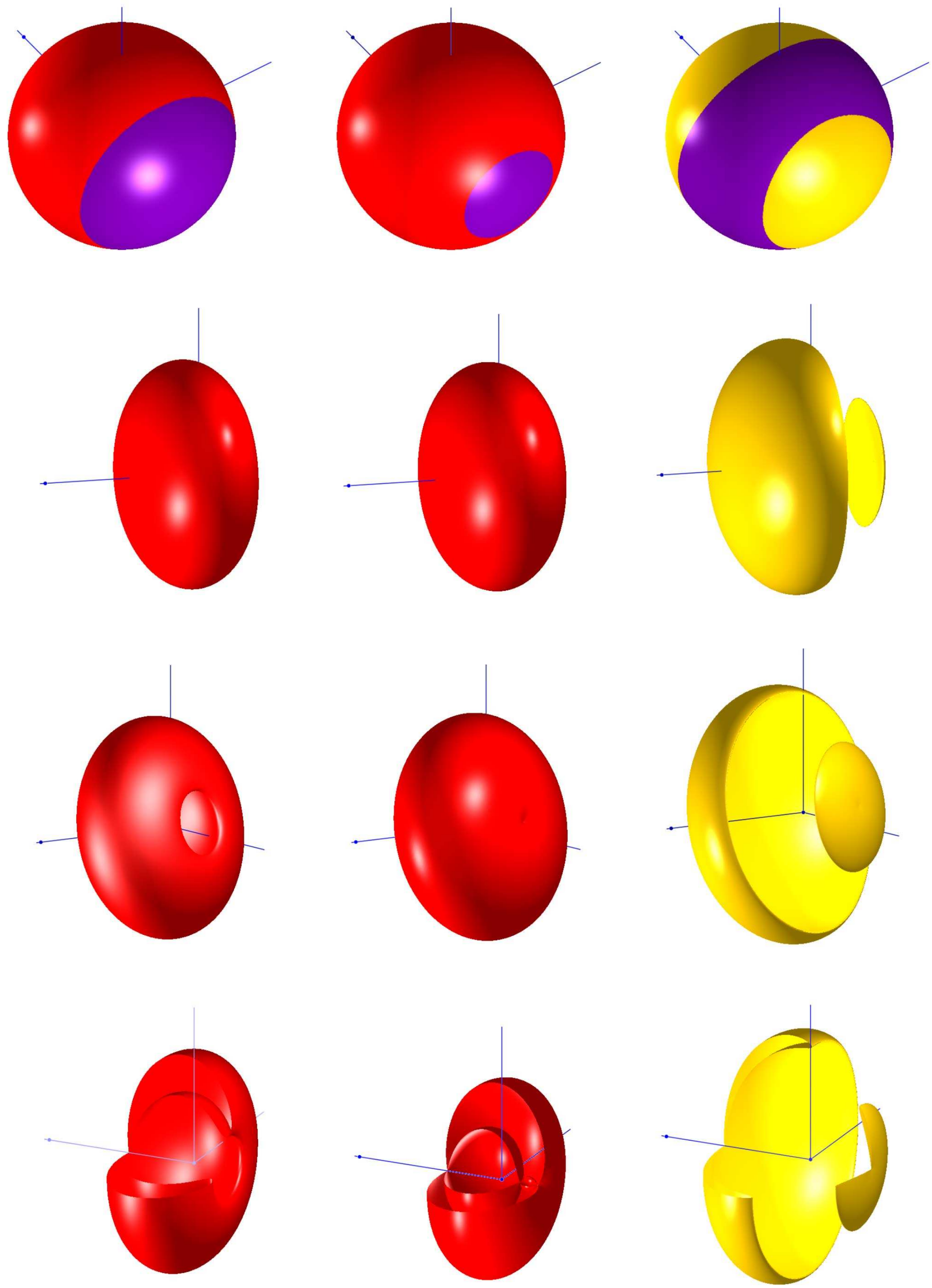

Fig. 18. Enveloping surfaces of types I: $(h, l) = (1, 1)$ (left), I$'$: $(h, l) = (1, 0.6)$ (middle), II: $(h, l) = (2.5, 2.15)$ (right).

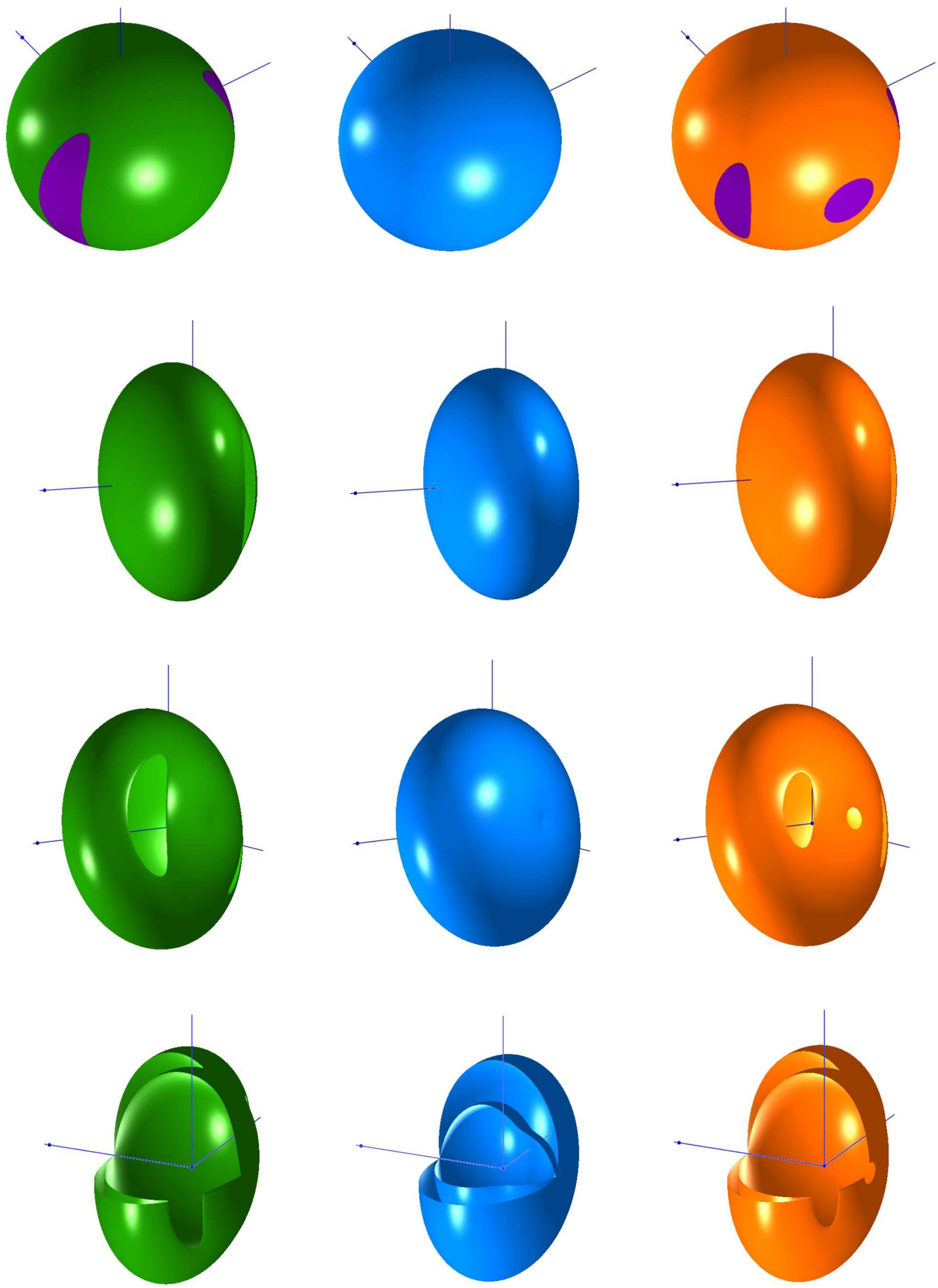

Fig. 19. Enveloping surfaces of types III: $(h, l) = (2, 1.8)$ (left), IV: $(h, l) = (1.5, 0.6)$ (middle), V: $(h, l) = (1.85, 1.705)$ (right).

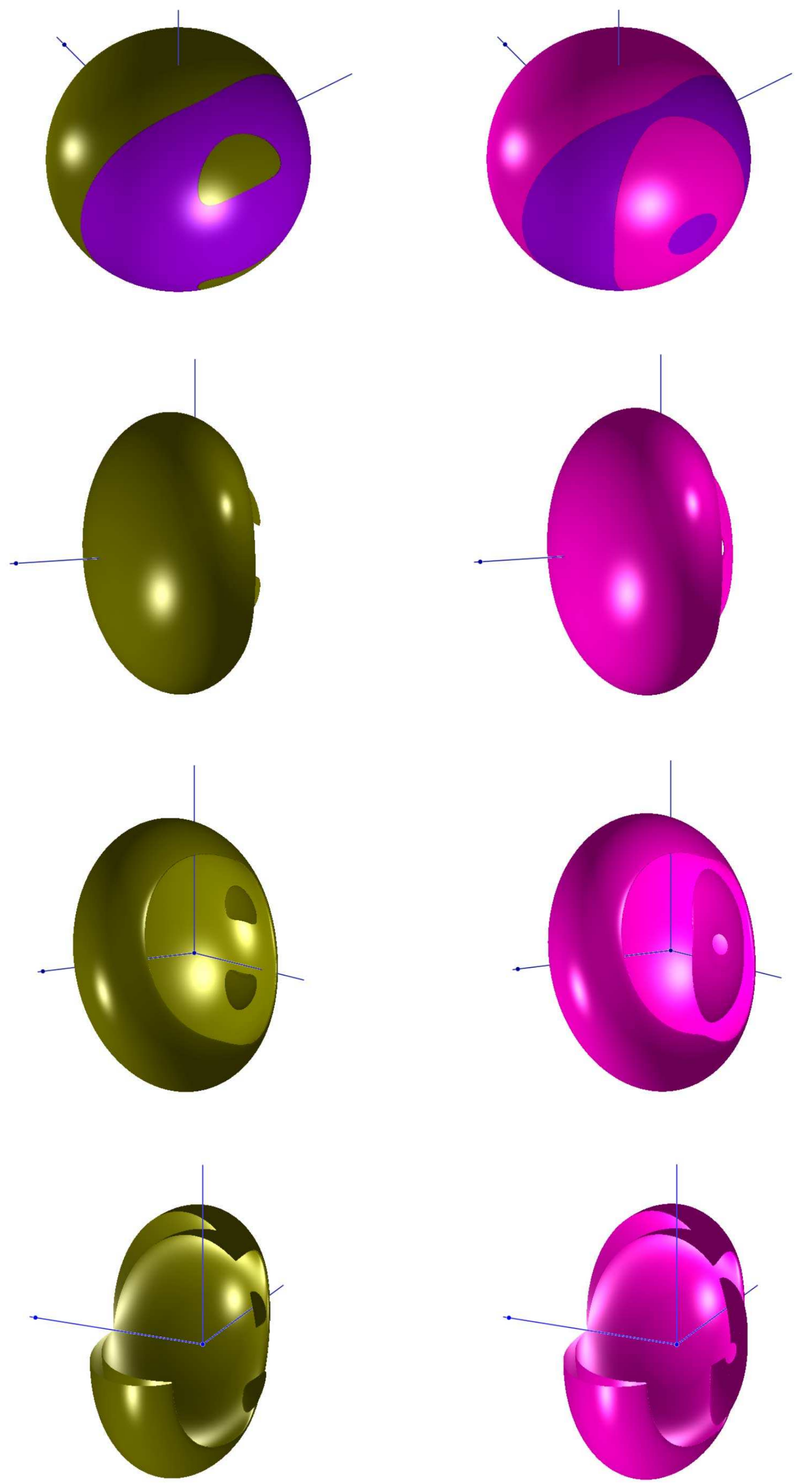

Fig. 20. Enveloping surfaces of types VI: $(h,\, l) = (1.9,\, 1.759)$ (left) and VII: $(h,\, l) = (1.912,\, 1.763)$ (right).

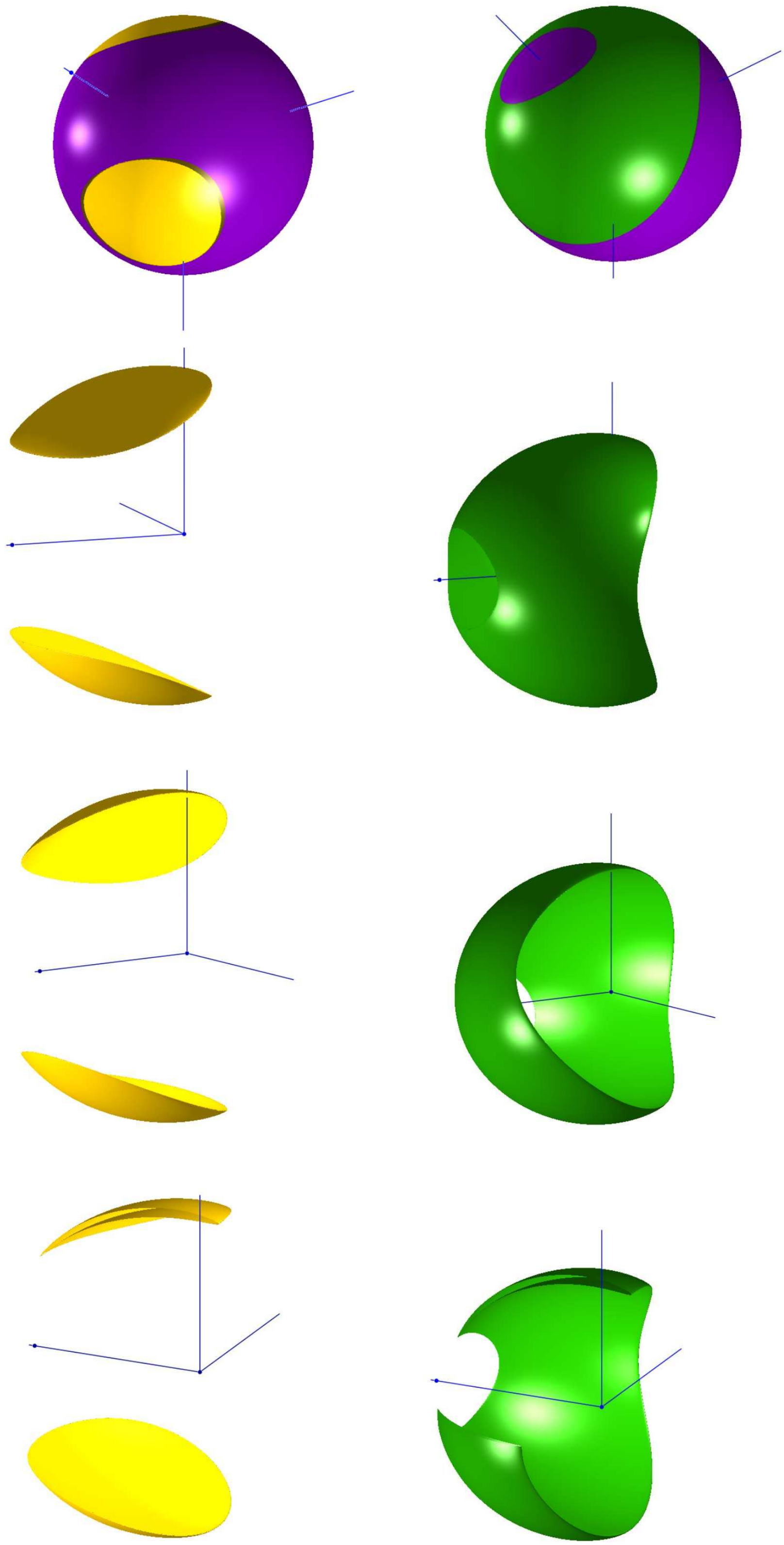

Fig. 21. Enveloping surfaces of types II$'$: $(h, l) = (3.6, 2.8)$ (left) and III$'$: $(h, l) = (3.6, 2.75)$ (right).

(c) *the classification of possible types of the enveloping surfaces $\partial\mathcal{V}_{h,l}$ is determined by the bifurcation set $\tilde{\Sigma} \subset \mathbb{R}^2(h, l)$ and the curve (49).*

For illustration, Figs. 18 to 21 give a complete survey on the types of enveloping surfaces that occur in the Katok family of rigid bodies, cf. Sec. 5. Each individual case is represented by a column of four images. At the top we show the Poisson sphere $S^2(\boldsymbol{\gamma})$; its colored part is $\tilde{\mathcal{U}}_{h,l}$ whereas the dark violet part is not covered by the projection of $\mathcal{P}^2_{h,l}$. The three pictures below give different views of the corresponding surface $\partial\mathcal{V}_{h,l}$. The dot on the $\mathbf{e} = \hat{\mathbf{r}}$ axis identifies the orientation. The bottom picture shows the envelope with one quarter cut away; this permits a view to the interior which is filled with $\mathcal{V}_{h,l}$, the domain of possible values $\boldsymbol{\omega}$. But remember each point of this interior has two pre-images in $\mathcal{E}^3_{h,l}$, one with increasing, the other with decreasing value of $\mathbf{l}^2$.

The first three Figs. 18 to 20 show the types of envelopes that occur in the Katok region K1, see Fig. 13. The parameters are $A = (1.7, 0.9, 0.86)$ and $\mathbf{r} = (1, 0, 0)$. The two cases I and I$'$ in Fig. 18 differ in the number $\nu(\partial\mathcal{V}_{h,l})$ of singularities; to the left of line (49) it is 1, to the right it is 3. In Fig. 21 we add the two additional possible cases for types II and III, cf. Table 2. They are the only enveloping surfaces without singular points. Type II$'$ occurs in the Katok parameter regions K4, K6 and K7; our choice is $A = (0.8, 1.1, 0.9) \in$ K7. Type III$'$ occurs only in K7; we take $A = (0.8, 1.1, 1.0)$. The values of (h, l) are indicated in the captions.

We add a remark on the structure induced in $\mathcal{E}^3_{h,l}$ by the pre-image $p^{-1}(\partial\mathcal{V}_{h,l}) = \mathcal{P}^2_{h,l}$. Any connected component of $\mathcal{P}^2_{h,l}$ is a two-dimensional oriented manifold which divides the corresponding nonsingular component of $\mathcal{E}^3_{h,l}$ into two oriented manifolds with boundary. It is known that any closed oriented three-dimensional manifold can be presented as the disjoint union of two filled-in manifolds of suitable genus, without common interior points; i.e. it is always possible to find $\mathcal{M}, \mathcal{M}' \subset \mathcal{E}^3_{h,l}$ such that $\mathcal{M} \cup \mathcal{M}' = \mathcal{E}^3_{h,l}$ and $\mathcal{M} \cap \mathcal{M}' = \partial\mathcal{M} = \partial\mathcal{M}'$. For example, the sphere S^3 can be obtained by pasting together two balls, up to the homeomorphism of their boundaries; by pasting two full tori it is possible to obtain manifolds S^3, $\mathbb{R}P^3$, $S^1 \times S^2$. Such splitting is called *Heegaard splitting* of genus n, where n is the topological genus of the manifold $\partial\mathcal{M}$. In the problem under consideration the surface $\partial\mathcal{M}$ is a connected component of $\mathcal{P}^2_{h,l} \subset \mathcal{E}^3_{h,l}$. The sets $\mathcal{M}$ and $\mathcal{M}'$ correspond to the parts of $\mathcal{E}^3_{h,l}$ where the signs of ζ_3 in (19) or of $d|A\boldsymbol{\omega}|^2/dt$ in (27) are different.

The trajectories $\boldsymbol{\omega}(t)$ fill in the closed domain $\mathcal{V}_{h,l}$ and are tangent to the enveloping surface $\partial\mathcal{V}_{h,l} \subset \mathbb{R}^3(\boldsymbol{\omega})$. Lifted to the energy surface, this tangency becomes a crossing-over between $\mathcal{M}$ and $\mathcal{M}'$, at almost all points of $\mathcal{P}^2_{h,l}$. But the trajectories cannot all be directed to the interior of $\mathcal{M}$ (or $\mathcal{M}'$). Therefore we may identify open disjoint domains on $\mathcal{P}^2_{h,l}$ with a different direction of the flow, from $\mathcal{M}$ to $\mathcal{M}'$ or vice versa. According to (27), the function $|A\boldsymbol{\omega}|$ attains a local extremum upon contact with $\mathcal{P}^2_{h,l}$. So one part of $\mathcal{P}^2_{h,l}$ consists of local minima of $|A\boldsymbol{\omega}|$, the other of local maxima. We find the separatrix from the condition $d^2|A\boldsymbol{\omega}|^2/dt^2 = 0$. In explicit terms, this condition reads

$$|\boldsymbol{\gamma} \times \mathbf{r}|^2 + \langle A\boldsymbol{\omega} \times \boldsymbol{\gamma}, \mathbf{r} \times \boldsymbol{\omega}\rangle = 0. \tag{51}$$

If $d^3|A\boldsymbol{\omega}|^2/dt^3 \neq 0$ at a point of this separatrix, the trajectory, after contact with $\mathcal{P}^2_{h,l}$, returns to the initial set $\mathcal{M}$ or $\mathcal{M}'$.

As mentioned in the Introduction, these observations are relevant for studying the dynamics in terms of global Poincaré sections. The surfaces $\mathcal{P}^2_{h,l}$ fulfill the requirement of being *complete* surfaces of section, a goal which is not always easy to obtain [Dullin & Wittek, 1995]. Their projections $\partial\mathcal{V}_{h,l}$ to the space of angular velocities are a natural choice for representing the motion, and we propose to use them in comprehensive studies of rigid body dynamics. The projections $\tilde{\mathcal{U}}_{h,l}$ to the Poisson sphere may also be used, but then to obtain a unique Poincaré mapping, only one of the two sheets associated with the two signs in Eq. (36) must be taken.

Acknowledgement

We thank Holger R. Dullin for many illuminating discussions.

References

Abraham, R. & Marsden, J. E. [1978] *Foundations of Mechanics* (Benjamin-Cummings, Reading MA).

Ampère, A. M. [1821] "Mémoire sur quelques nouvelles propriétés des axes permanents de rotatione des corps et des plans directeurs de ces axes," *Mém. de l'Acad. Scient. Paris* **5**, 86–152.

Appelrot, G. G. [1940] "Not entirely symmetrical heavy gyroscopes," in *Rigid Body Motion About a*

Fixed Point, *Collection of Papers in Memory of S. V. Kovalevskaya* (Acad. Sci. USSR, Dept. of Technical Sciences, Moscow, Leningrad), pp. 61–155 (in Russian).

Arkhangelskii, Yu. A. [1977] *Analytical Dynamics of a Rigid Body* (Nauka, Moscow) (in Russian).

Arnold, V. I. [1974] *Mathematical Methods of Classical Mechanics* (Nauka, Moscow) (in Russian); Engl. transl. [1978] (Springer-Verlag, NY).

Arnold, V. I., Kozlov, V. V. & Neishtadt, A. I. [1985] *Mathematical Aspects of Classical and Celestial Mechanics* (VINITI, Moscow) (in Russian); Engl. transl. [1988] *Dynamical Systems III*, ed. Arnold, V. I. (Springer-Verlag, NY).

Bobenko, A. I., Reyman, A. G. & Semenov-Tian-Shansky, M. A. [1989] "The Kowalewski top 99 years later: A lax pair, generalizations and explicit solutions," *Commun. Math. Phys.* **122**, 321–354.

Bolsinov, A. V., Dullin, H. R. & Wittek, A. [1996] "Topology of energy surfaces and existence of transversal Poincaré section," *J. Phys.* **A29**, 4977–4985.

Bolsinov, A. V. & Fomenko, A. T. [1999] *Integrable Hamiltonian Systems. Geometry, Topology, Classification* (Udm. University, Izhevsk) (in Russian).

Bolsinov, A. V., Richter, P. H. & Fomenko, A. T. [2000] "The method of loop molecules and the topology of the Kovalevskaya top," *Matem. Sbornik* **191**, 3–42 (in Russian); Engl. transl. *Sbornik: Mathematics* **191**, 151–188.

Dovbysh, S. A. [1990] "Splitting of separatrices of unstable uniform rotations and non-integrability of a perturbed Lagrange problem," *Vestnik Moskov. Univ., Ser. Mat. Mekh.* **3**, 70–77 (in Russian).

Dullin, H. R. [1994] *Die Energieflächen des Kowalewskaja-Kreisels*, Dissertation Univ. Bremen (Mainz Verlag, Aachen).

Dullin, H. R., Juhnke, M. & Richter, P. H. [1994] "Action integrals and energy surfaces of the Kovalevskaya top," *Int. J. Bifurcation and Chaos* **4**, 1535–1562.

Dullin, H. R. & Wittek, A. [1995] "Complete Poincaré sections and tangent sets," *J. Phys.* **A28**, 7157–7180.

Dullin, H. R., Richter, P. H. & Veselov, A. P. [1998] "Action variables of the Kovalevskaya top," *Reg. Chaotic Dyn.* **3**, 18–31.

Gashenenko, I. N. [2000] "Angular velocity of the Kovalevskaya top," *Reg. Chaotic Dyn.* **5**, 104–113.

Golubev, V. V. [1953] *Lectures on Integration of the Equations of Motion of a Rigid Body About a Fixed Point* (Gostekhizdat, Moscow) (in Russian); Engl. transl. [1960] (Jerusalem).

Gorr, G. V. & Iljukhin, A. A. [1974] "Cases of constancy of the modulus of the angular momentum of a gyrostat," *Mekh. Tverd. Tela, Kiev: Naukova dumka* **6**, 9–15 (in Russian).

Grioli, G. [1947] "Essistenza e determinazione delle precessioni regolari dinamicamente possibli per un solido pesante asimmetrico," *Ann. Matem.* **26**, 271–281.

Hess, W. [1890] "Über die Euler'schen Bewegungsgleichungen und über eine neue particuläre Lösung des problems der Bewegung eines starren Körpers um einen festen Punkt," *Math. Ann.* **37**, 153–181.

Iacob, A. [1971] "Invariant manifolds in the motion of a rigid body about a fixed point," *Rev. Roum. Math. Pures et Appl.* **16**, 1497–1521.

Katok, S. B. [1972] "Bifurcation sets and integral manifolds in the problem of motion of a heavy rigid body," *Usp. Math. Nauk* **27**, 126–132 (in Russian).

Kharlamov, M. P. [1988] *The Topological Analysis of Integrable Problems of Rigid Body Dynamics*, (Leningrad University) (in Russian).

Kharlamov, P. V. [1965] *Lectures on Dynamics of a Rigid Body* (Novosibirsk University) (in Russian).

Klein, F. & Sommerfeld, A. [1910] *Über die Theorie des Kreisels* (Teubner-Verlag, Leipzig).

Kötter, F. [1893] "Sur le cas traité par M^{me} Kowalevski de rotation d'un corps solide autour d'un point fixe," *Acta Math.* **17**, 209–264.

Kowalevski, S. [1890] "Mémoire sur un cas particulier du problème de la rotation d'un corps pesant autour d'un point fixe, où l'integration s'effectue à l'aide de fonctions ultraelliptiques du temps," *Acad. des Sciences de l'Institut de France. Mémoires présentés par divers savants* **31**, 1–62.

Kozlov, V. V. [1980] *Methods of Qualitative Analysis in the Dynamics of a Rigid Body* (Moscow University) (in Russian).

Kozlov, V. V. [1995] *Symmetry, Topology, and Resonances in Hamiltonian Mechanics* (Udm. University, Izhevsk) (in Russian).

Kuznetzov, V. B. & Nijhoff, F. W. (eds.) [2001] *Special issue*: *Papers Based on the Kowalewski Workshop on Mathematical Methods of Regular Dynamics*, April 2000, University of Leeds, UK, *J. Phys. A Math. Gen.* **34**.

Landau, L. D. & Lifshitz, E. M. [1958] *Mechanics* (Phyzmathgiz, Moscow) (in Russian); Engl. transl. [1984] (Pergamon Press, Oxford, NY).

Lewis, D., Ratiu, T., Simo, J. C. & Marsden, J. E. [1992] "The heavy top: A geometric treatment," *Nonlinearity* **5**, 1–48.

Lyapunov, A. M. [1954] "On one property of the differential equations of the problem of the motion of a heavy rigid body having a fixed point," *Coll. Works* (AS USSR, Moscow), Vol. 1, pp. 402–417 (in Russian).

McCord, C. K., Meyer, K. R. & Wang, Q. [1998] *The Integral Manifolds of the Three Body Problem*, Memoirs of the AMS, Vol. 132, No. 628, pp. 1–91.

Milnor, J. [1963] *Morse Theory* (Princeton University).

Oshemkov, A. A. [1991] "Fomenko invariants for the main integrable cases of the rigid body motion equations," *Adv. Sov. Math.* **6**, 67–146.

Poincaré, H. [1892–1899] *Les Méthodes Nouvelles de la Mécanique Céleste*, t. 1–3 (Gauthier-Villars, Paris).

Richter, P. H., Dullin, H. R. & Wittek, A. [1997] "Kovalevskaya top," *Publ. Wiss. Film. C1961*, *Sek. Techn. Wiss./Naturwiss.* **13**, 33–96.

Routh, E. J. [1884] *Advanced Rigid Dynamics* (*The Advanced Part of a Treatise on the Dynamics of a System of Rigid Bodies*) (McMillan, London).

Smale, S. [1970] "Topology and mechanics I," *Invent. Math.* **10**, 305–331; "Topology and mechanics II," *Invent. Math.* **11**, 45–64.

Staude, O. [1894] "Über permanente Rotationsaxen bei der Bewegung eines schweren Körpers um einen festen Punkt," *J. Reine und Angew. Math.* **113**, 318–334.

Tatarinov, Ya. V. [1973] "Phase topology of compact configurations with symmetry," *Vestnik Moskov. Univ., Ser. Mat. Mekh.* **5**, 70–77 (in Russian).

Tatarinov, Ya. V. [1974] "Portraits of classical integrals in the problem on rotation of a rigid body about a fixed point," *Vestnik Moskov. Univ., Ser. Mat. Mekh.* **6**, 99–105 (in Russian).

Whittaker, E. T. [1964] *A Treatise on the Analytical Dynamics of Particles and Rigid Bodies* (Cambridge University).

Zhukovskii, N. E. [1896] "Geometric interpretation of the case considered by Kovalevskaya of the motion of a heavy rigid body about a fixed point," *Mat. Sbornik* **19**, 45–93 (in Russian).

Ziglin, S. L. [1983] "Branching of solutions and nonexistence of first integrals in Hamiltonian mechanics II," *Funct. Anal. Appl.* **17**, 8–23 (in Russian).